Redox Biology 46 (2021) 102093

Contents lists available at ScienceDirect

Redox Biology

journal homepage: www.elsevier.com/locate/redox

Quantitative trait mapping in Diversity Outbred mice identifies novel genomic regions associated with the hepatic glutathione redox system

Rebecca L. Gould [a], Steven W. Craig [a], Susan McClatchy [b], Gary A. Churchill [b], Robert Pazdro [a,*]

[a] Department of Nutritional Sciences, University of Georgia, 305 Sanford Drive, Athens, GA, 30602, USA
[b] The Jackson Laboratory, 600 Main Street, Bar Harbor, ME, 04609, USA

ARTICLE INFO

Keywords:
Liver
Glutathione
Redox
Genetics
QTL mapping

ABSTRACT

The tripeptide glutathione (GSH) is instrumental to antioxidant protection and xenobiotic metabolism, and the ratio of its reduced and oxidized forms (GSH/GSSG) indicates the cellular redox environment and maintains key aspects of cellular signaling. Disruptions in GSH levels and GSH/GSSG have long been tied to various chronic diseases, and many studies have examined whether variant alleles in genes responsible for GSH synthesis and metabolism are associated with increased disease risk. However, past studies have been limited to established, canonical GSH genes, though emerging evidence suggests that novel loci and genes influence the GSH redox system in specific tissues. The present study marks the most comprehensive effort to date to directly identify genetic loci associated with the GSH redox system. We employed the Diversity Outbred (DO) mouse population, a model of human genetics, and measured GSH and the essential redox cofactor NADPH in liver, the organ with the highest levels of GSH in the body. Under normal physiological conditions, we observed substantial variation in hepatic GSH and NADPH levels and their redox balances, and discovered a novel, significant quantitative trait locus (QTL) on murine chromosome 16 underlying GSH/GSSG; bioinformatics analyses revealed *Socs1* to be the most likely candidate gene. We also discovered novel QTL associated with hepatic $NADP^+$ levels and $NADP^+$/NADPH, as well as unique candidate genes behind each trait. Overall, these findings transform our understanding of the GSH redox system, revealing genetic loci that govern it and proposing new candidate genes to investigate in future mechanistic endeavors.

1. Introduction

Glutathione is a ubiquitous and versatile intracellular antioxidant [1]. A tripeptide comprised of glycine, glutamate, and cysteine, its biochemical functions are mediated by a sulfhydryl group on the cysteine residue [2]. In the cell, glutathione mostly exists in its reduced thiol form (GSH), and enzymes such as glutathione peroxidase (GPx) and glutaredoxins convert it to the dimer glutathione disulfide (GSSG), which is recycled back to two molecules of GSH via NADPH-dependent glutathione reductase (GR) [1,3]. Though GSH and GSSG are in a constant state of flux, their levels – and the ratio GSH/GSSG, or 2GSH/GSSG – provide an informative glimpse into the redox environment of the cell and shifts in these values often indicate oxidative stress [1,4]. Furthermore, decreases in tissue GSH levels and GSH/GSSG, and corresponding increases in GSSG levels, have been observed in a wide array of chronic diseases including liver disease [5,6], chronic kidney disease [7,8], heart disease [9,10], diabetes mellitus [11–13], and obesity [14].

Because of the close relationship between GSH and chronic diseases, many studies have sought to determine whether variant alleles in genes encoding GSH-related enzymes, including GPx and GR, predict chronic disease risk in human populations. *GPX1* polymorphisms have been associated with increased risk of breast cancer [15,16], chronic kidney disease [17], prostate cancer [18], coronary artery disease [19], acute myeloid leukemia [19], and diabetes-related kidney complications [20]. Moreover, variants in *GPX* isoforms have been associated with risk for arterial ischemic stroke in young adults and children (*GPX3*) [21] and prepubertal childhood obesity (*GPX4, 5,* and *6*) [22], though these trends have not been consistent across all populations [23–28]. Other studies have examined the disease relevance of polymorphisms in genes involved in glutathione biosynthesis, notably glutathione cysteine ligase (GCL) and glutathione synthetase (GS), which directly affect cellular GSH concentrations [29]. Polymorphisms in the catalytic subunit of GCL (*GCLC*) have been associated with cystic fibrosis [30], chronic obstructive pulmonary disease [31], pulmonary tuberculosis [32], drug

* Corresponding author.
E-mail address: rpazdro@uga.edu (R. Pazdro).

https://doi.org/10.1016/j.redox.2021.102093
Received 6 May 2021; Received in revised form 24 July 2021; Accepted 4 August 2021
Available online 5 August 2021

sensitivity in human tumor cell lines [33], methylmercury retention [34], vasomotor function and myocardial infarction [35,36]. Functional polymorphisms in the GCL modifier subunit (*GCLM*) have been linked with ischemic heart disease and vasomotor function [36,37], and in some cases, schizophrenia [38–40]. Lastly, polymorphisms in *GS* have been associated with susceptibility to lung dysfunction and lung cancer, as well as patient survival [41,42]. Mutations in these genes have also been found in patients with inborn errors in glutathione metabolism, though the diseases are rare [43–47].

While most genetics studies have focused on core genes with established functions in GSH biosynthesis and metabolism, emerging evidence suggests that novel loci and genes impact tissue GSH dynamics as well. Multiple studies have shown that GSH and GSSG levels and GSH/GSSG are heritable in mice [48–52] and humans [53] alike, and Zhou et al. discovered new genetic loci associated with hepatic GSH levels and GSH/GSSG in mice [51]. However, those genes were found using a panel of inbred mouse strains, which do not fully reflect the human condition, and many *in silico* mapping tools have limited power and a predisposition toward false positives [54–56]. Thus, more powerful and comprehensive approaches are needed to identify genes that truly govern tissue GSH levels and redox balance, and ultimately, affect chronic disease risk.

In the present study, we performed genome-wide analysis of hepatic GSH and GSSG levels, as well as GSH/GSSG, in the Diversity Outbred (DO) mouse stock, which models the genetic diversity of humans and facilitates high-precision mapping of quantitative trait loci (QTL) [57,58]. To best understand the genetics of the entire GSH system [59], we expanded our analysis to include the redox cofactor NADPH, which is essential for GSH recycling [60], and its precursor NADH. To our knowledge, this is the most comprehensive genetic mapping study to focus on tissue GSH homeostasis, and overall, our results point to novel loci and candidate genes that will vastly expand our understanding of this essential redox system and its regulation.

2. Materials and methods

2.1. Mice

Male and female Diversity Outbred (DO) mice (J:DO; JAX® #009376) from generations 30, 32, and 35 were purchased from The Jackson Laboratory (Bar Harbor, ME USA); the DO stock was originally generated from eight inbred founder strains: A/J (AJ), C57BL/6J (B6), 129S1/SvImJ (129), NOD/ShiLtJ (NOD), NZO/HlLtJ (NZO), CAST/EiJ (CAST), PWK/PhJ (PWK), and WSB/EiJ (WSB). All mice arrived at 4 weeks of age and were given *ad libitum* access to water and standard chow diet (LabDiet®, St. Louis, MO USA, product 5053) and kept on a 12 h light-dark cycle. These conditions were maintained until the mice were sacrificed at 5–6 months of age. Prior to sacrifice, and during the light cycle, all mice were fasted for 3–4 h. Then mice were humanely euthanized by cervical dislocation and tissues were collected for analysis. A total of 351 mice (174 males, 177 females) were sacrificed, and at the time of harvest, total body weight (g), liver weight (g), and liver weight/body weight (%) were documented (Supplementary Tables S1–S3; Supplementary Figure S1). The University of Georgia Institutional Animal Care and Use Committee (IACUC) approved all methods and procedures involving animals in accordance with the ethical standards of the institution (AUP #A2016-07-016), and all methods and procedures were carried out in accordance with the National Institutes of Health guide for the care and use of Laboratory animals (NIH Publications No. 8023, revised 1978).

2.2. Assessment of hepatic total glutathione, GSH, GSSG, and redox ratios

Samples of liver tissue were promptly harvested from each mouse after humane euthanasia. Tissues were rinsed with ice-cold PBS, promptly blotted on a paper towel, and flash frozen in liquid nitrogen. Within 12 h of each harvest, samples were homogenized in PBS containing 10 mM diethylenetriaminepentaacetic acid (DTPA) and promptly acidified with an equal volume of ice-cold 10% perchloric acid (PCA) containing 1 mM DTPA as previously described [52,61]. Acidified samples underwent centrifugation (15,000 RPM at 4C for 15 min) and the acidified supernatant was collected and filtered. Filtered supernatant samples were stored at −80°C until analysis, and all samples were analyzed within 6 months. GSH and GSSG concentrations were quantified in each sample by HPLC coupled with electrochemical detection (Dionex Ultimate 3000, Thermo Fisher Scientific, Waltham, MA USA) based on previously published methods [61]. A conditioning cell was set to +500 mV and placed immediately before the boron-doped diamond cell which was set at +1475 mV with a cleaning potential at +1900 mV between samples. The mobile phase consisted of 4.0% acetonitrile, 0.1% pentafluoropropionic acid, and 0.02% ammonium hydroxide. The flow rate was maintained at 0.22 mL/min and injection volumes were set at 5.0 μL. Peaks were quantified using external GSH and GSSG standards, external calibration, and the Chromeleon Chromatography Data System Software (Dionex Version 7.2, Thermo Fisher Scientific, Waltham, MA USA). Total glutathione concentrations were determined by calculating $[GSH] + [2GSSG]$ and all glutathione concentrations were standardized to total protein (Pierce BCA Protein Assay, Thermo Fisher Scientific, Waltham, MA USA) and expressed in nmol/mg protein. The ratio of GSH/GSSG was then calculated. Another commonly reported measurement related to GSH dynamics and oxidative stress is the redox potential E_h of the redox couple [62–67]. To calculate the redox potential (E_h) of the GSSG-GSH pair ($2GSH \rightarrow GSSG + 2e^- + 2H^+$) in each liver sample, we used the Nernst equation at 40 °C:

$$E_h = E_0 + \frac{RT}{nF}\ln\left[\frac{(ox)}{(red)}\right]$$

E_h = measured cell potential, E_0 = standard electrode potential for GSSG/2GSH (−264 mV at pH 7.4 [63–65]), R = gas constant (8.3145 J x mol^{-1} x K^{-1}), T = temperature in Kelvin (313.15 K), n = number of electrons transferred (2), F = Faraday's constant (96485C x mol^{-1}), ox = molar concentration of oxidant (GSSG), and red = molar concentration of reductant (GSH). The exponential of GSH reflects the stoichiometry where 2 GSH are oxidized per 1 GSSG formed [62]. Tissue concentrations of GSH and GSSG (nmol/mg protein) were expressed in molar concentrations [66,67] using a conversion factor of 500 μL/mg of protein. The final equation used to calculate E_h (mV) for the GSSG-GSH couple was:

$$E_h(mV) = -264 + 31\log\left[\frac{(GSSG)}{(GSH)^2}\right]$$

2.3. Assessment of hepatic NADPH, NADP$^+$, NADP$^+$/NADPH, and NADH

Liver samples collected at harvest were rinsed with ice-cold PBS, blotted on a paper towel, and flash frozen in liquid nitrogen. Within 12 h of each harvest, samples were homogenized, processed, and analyzed by kit (NADP/NADPH Quantification Kit and NAD/NADH Quantification Kit, MilliporeSigma, Burlington, MA USA) according to the manufacturer's instructions. All nicotinamide adenine dinucleotide (NAD) phenotypes were standardized to total protein (Pierce BCA Protein Assay, Thermo Fisher Scientific, Waltham, MA USA) and expressed in pmol/μg protein.

2.4. Genotyping

Genotyping was performed on all 351 DO samples. DNA was extracted from tail tips collected at sacrifice and subsequently genotyped using the third-generation Mouse Universal Genotyping Array (GigaMUGA) [68] performed by GeneSeek (Neogen Genomics, Lincoln,

Table 1
Descriptive statistics for hepatic redox system metabolites in DO mice.

Phenotype	N	$\bar{x}$	Median	SD	Min	Max
Total Glutathione (nmol/mg)	346	45.945	43.045	19.215	10.183	117.232
GSH (nmol/mg)	346	44.695	41.971	18.708	9.843	113.359
GSSG (nmol/mg)	347	0.627	0.558	0.346	0.140	2.288
GSH/GSSG	346	78.052	74.714	25.120	31.894	177.181
E_h (mV)	346	−195.278	−195.477	7.707	−215.556	−166.948
NADPH (pmol/μg)	335	0.262	0.238	0.170	0.011	0.898
$NADP^+$ (pmol/μg)	331	0.981	0.890	0.450	0.157	2.575
$NADP^+$/NADPH	319	9.888	3.694	19.499	0.460	161.363
NADH (pmol/μg)	332	2.788	2.788	1.233	0.293	7.572

NE USA, 68504). This 143K-probe array is built on the Illumina Infinium II platform and has been optimized for genetic mapping in the DO populations.

2.5. Quantitative trait loci (QTL) mapping

Genome scans were performed using 347 (172 male, 175 female) of the original 351 DO samples; 2 mice were excluded from QTL analysis because they were XO females, and 2 were excluded due to low call rates. Prior to analysis, all phenotypic data underwent *z*-score transformation to ensure normality [69]. We then performed genomes scans using R/qtl2 software [58], and for each phenotype, scans included sex and experimental cohort as additive covariates. Each genome scan model also accounted for kinship among the DO mice using the "leave one chromosome out" (LOCO) method [58,70]. Significance thresholds were determined for individual traits by performing 1000 permutations [58,71,72], and we applied a suggestive threshold (p-value≤0.20) for reporting QTL loci based on the permutation analysis [72]. A 95% Bayesian credible interval was calculated around each peak using the R/qtl2 *find_peaks* and *bayes_int* functions [58,71]. To estimate allelic contributions of the eight founder strains at specific QTL, we used the Best Linear Unbiased Predictors (BLUPs) model within R/qtl2 [73]. Genes within Bayesian credible intervals ±1 Mbp were plotted using R/qtl2 via connection with the Mouse Genome Informatics (MGI) database. All genotype data, genotype probabilities, and marker information are publicly available through figshare (https://doi.org/10.6084/m9.figshare.c.5360501.v1). All source code, phenotype data, and other files used in QTL analyses are available through a public GitHub repository (https://doi.org/10.5281/zenodo.4683881).

2.6. Candidate gene analysis

To interrogate the plausibility of candidate genes within significant and suggestive loci, we used an integrative bioinformatics approach that queried databases for expression, phenotypic, and functional annotations based on previously published methods [74,75]. First, we identified all protein-coding and functional RNA genes within the significant QTL intervals ±1 Mbp reported by R/qtl2 using the Unified Mouse

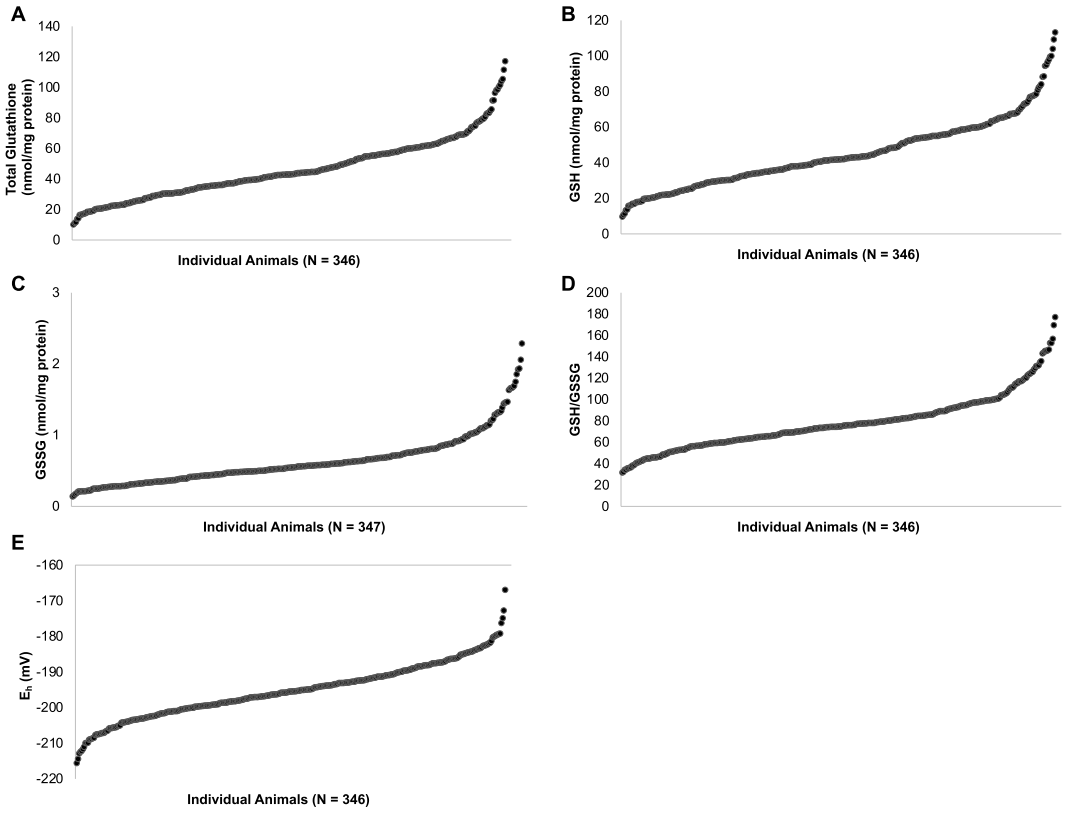

Fig. 1. Variation in hepatic glutathione concentrations and redox balance in the DO population. Hepatic concentrations of **A.** Total Glutathione (GSH+2GSSG, expressed in nmol/mg); **B.** GSH (nmol/mg); **C.** GSSG (nmol/mg); **D.** GSH/GSSG; and **E.** Redox Potential of the GSSG-GSH couple, indicated as E_h (mV) were measured in a population of DO mice. Values are arranged from smallest to largest, and the N for each measurement is provided underneath each panel.

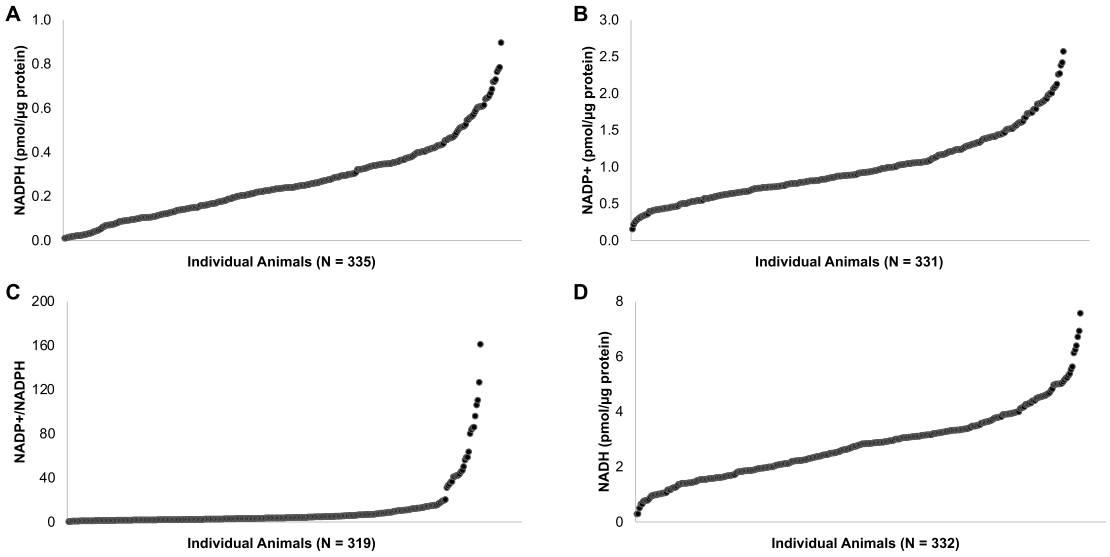

Fig. 2. Variation in hepatic NAD(P)H concentrations and redox balances in the DO population. Hepatic concentrations of **A.** NADPH (pmol/µg); **B.** $NADP^+$ (pmol/µg); **C.** $NADP^+$/NADPH; and **D.** NADH (pmol/µg) in a population of DO mice. Values are arranged from smallest to largest, and the N for each measurement is provided underneath each panel.

Genome Feature Catalog within the Mouse Genome Informatics (MGI) database. Second, for each genome feature in the region, we compiled expression annotations from the bioinformatics resources listed in Supplementary Table S4. Gene expression annotations were collected from the EBI Expression Atlas (EEA) [76] and the Gene eXpression Database (GXD) [77] through MGI [78]. Functional annotations were collected using InterPro [79] and Gene Ontology (GO) annotations [80, 81] obtained through MGI [78]. All phenotypic data relevant to the liver were collected from PheWeb [82] and Ensembl BioMart [83].

2.7. Statistical analysis

IBM SPSS Statistics version 26 (SPSS Inc., Chicago, IL USA) was used to detect the significance of relationships between variables of interest. Mann-Whitney tests were used to compare variables between sex to elucidate any sex-effects between variables, and the test included a U statistic and a standard error. RStudio version 1.3.1093 (RStudio, PBC., Boston, MA USA) and R version 4.0.2 (R Foundation for Statistical Computing, Vienna, Austria) were used to evaluate correlations between values and rank-based Spearman's rho (ρ) was calculated for each relationship. A relationship between variables was considered statistically significant if the p-value was less than 0.05.

3. Results

3.1. Hepatic GSH and NADPH vary significantly among outbred mice

In a large cohort of genetically-diverse DO mice, we measured hepatic concentrations of GSH and GSSG, as well as GSH/GSSG, and found that under normal physiological conditions, these phenotypes vary widely (Table 1; Fig. 1). Hepatic concentrations of total glutathione and GSH exhibited an over 11-fold difference, ranging from 10.183 to 117.232 nmol/mg and 9.843 to 113.359 nmol/mg, respectively. Hepatic GSSG concentrations ranged from 0.140 to 2.288 nmol/mg, reflecting a 16-fold difference, and GSH/GSSG ranged from 31.894 to 177.181, over a 5-fold difference. We observed a significant degree of variation in hepatic E_h with a range of −215.556 to −166.948 mV, a 1.3-fold difference. There were no sex effects observed for any of these phenotypes (Supplementary Tables S5 and S6).

A similar degree of variation was observed in the redox cofactor NADPH and its precursor NADH (Table 1; Fig. 2). $NADP^+$ concentrations ranged from 0.157 to 2.575 pmol/µg, over a 16-fold difference, while its reduced form NADPH ranged from 0.011 to 0.898 pmol/µg, over an 81-fold difference. $NADP^+$/NADPH ranged from 0.460 to 161.363, over a 350-fold difference. NADH ranged from 0.293 to 7.572 pmol/µg, over a 25-fold difference. Sex-specific values are found in Supplementary Tables S5 and S6.

We screened for statistical associations among variables and discovered multiple significant correlations. Association results are listed in Table 2 and shown visually in Fig. 3. Hepatic total glutathione concentrations were positively correlated with GSH concentrations ($\rho = 1.000$, $p = <0.001$), GSSG concentrations ($\rho = 0.801$, $p = <0.001$), and GSH/GSSG levels ($\rho = 0.120$, $p = 0.026$), and were strongly negatively correlated with E_h levels ($\rho = -0.799$, $p = <0.001$). Hepatic GSH concentrations were positively correlated with GSSG concentrations ($\rho = 0.791$, $p = <0.001$) and GSH/GSSG levels ($\rho = 0.137$, $p = 0.011$), and were negatively correlated with E_h levels ($\rho = -0.810$, $p = <0.001$). Hepatic GSSG concentrations were negatively correlated with GSH/GSSG levels ($\rho = -0.443$, $p = <0.001$) and E_h levels ($\rho = -0.326$, $p = <0.001$). Hepatic GSH/GSSG levels were negatively correlated with E_h levels ($\rho = -0.652$, $p = <0.001$).

Hepatic NADPH concentrations were positively correlated with total glutathione concentrations ($\rho = 0.265$, $p = <0.001$), GSH concentrations ($\rho = 0.267$, $p = <0.001$), and GSSG concentrations ($\rho = 0.203$, $p = <0.001$), and negatively correlated with $NADP^+$ concentrations ($\rho = -0.278$, $p = <0.001$), $NADP^+$/NADPH levels ($\rho = -0.846$, $p = <0.001$) and E_h levels ($\rho = -0.234$, $p = <0.001$). Hepatic $NADP^+$ concentrations were negatively correlated with total glutathione concentrations ($\rho = -0.306$, $p = <0.001$), GSH concentrations ($\rho = -0.306$, $p = <0.001$), GSSG concentrations ($\rho = -0.269$, $p = <0.001$), and $NADP^+$ concentrations ($\rho = -0.142$, $p = 0.010$), and positively correlated with $NADP^+$/NADPH levels ($\rho = 0.711$, $p = <0.001$) and E_h levels ($\rho = 0.226$, $p = <0.001$). Hepatic $NADP^+$/NADPH levels were positively correlated with E_h levels ($\rho = 0.240$, $p = <0.001$) and negatively correlated with total glutathione concentrations ($\rho = -0.296$, $p = <0.001$), GSH concentrations ($\rho = -0.297$, $p = <0.001$), and GSSG concentrations ($\rho = -0.233$, $p = <0.001$). Neither NADPH or $NADP^+$, nor the $NADP^+$/NADPH ratio were found to be correlated with GSH/GSSG ($p = 119$, $p = 0.850$, and $p = 0.208$, respectively). Hepatic NADH concentrations were positively correlated with NADPH ($\rho = 0.191$, $p = 0.001$), total glutathione

Table 2
Statistical relationships among markers of the hepatic GSH redox system as well as liver weights.
Spearman's rho (ρ) was calculated for each variable combination. Total glutathione, GSH, and GSSG concentrations were standardized as nmol/mg protein. Concentrations of NADPH, NADP, and NADH were standardized as pmol/μg protein. E_h was expressed as mV. Liver weight was reported in grams (g). * indicates a significant relationship (p≤0.05).

Variables	ρ	p-value
Total Glutathione, GSH	1.000*	<0.001
Total Glutathione, GSSG	0.801*	<0.001
Total Glutathione, GSH/GSSG	0.120*	0.026
Total Glutathione, E_h	−0.799*	<0.001
Total Glutathione, NADPH	0.265*	<0.001
Total Glutathione, $NADP^+$	−0.306*	<0.001
Total Glutathione, $NADP^+$/NADPH	−0.296*	<0.001
Total Glutathione, NADH	0.250*	<0.001
GSH, GSSG	0.791*	<0.001
GSH, GSH/GSSG	0.137*	0.011
GSH, E_h	−0.810*	<0.001
GSH, NADPH	0.267*	<0.001
GSH, $NADP^+$	−0.306*	<0.001
GSH, $NADP^+$/NADPH	−0.297*	<0.001
GSH, NADH	0.253*	<0.001
GSSG, GSH/GSSG	−0.443*	<0.001
GSSG, E_h	−0.326*	<0.001
GSSG, NADPH	0.203*	<0.001
GSSG, $NADP^+$	−0.269*	<0.001
GSSG, $NADP^+$/NADPH	−0.233*	<0.001
GSSG, NADH	0.123*	0.025
GSH/GSSG, E_h	−0.652*	<0.001
E_h, NADPH	−0.234*	<0.001
E_h, $NADP^+$	0.226*	<0.001
E_h, $NADP^+$/NADPH	0.240*	<0.001
E_h, NADH	−0.307*	<0.001
NADPH, $NADP^+$	−0.278*	<0.001
NADPH, $NADP^+$/NADPH	−0.846*	<0.001
NADPH, NADH	0.191*	0.001
$NADP^+$, $NADP^+$/NADPH	0.711*	<0.001
$NADP^+$, NADH	−0.142*	0.010
$NADP^+$/NADPH, NADH	−0.181*	0.001
Liver Weight, Total Glutathione	0.137*	0.011
Liver Weight, GSH	0.136*	0.012
Liver Weight, GSSG	0.176*	0.001
Liver Weight, GSH/GSSG	−0.089	0.099
Liver Weight, E_h	−0.050	0.349
Liver Weight, NADPH	0.203*	<0.001
Liver Weight, $NADP^+$	−0.218*	<0.001
Liver Weight, $NADP^+$/NADPH	−0.262*	<0.001
Liver Weight, NADH	−0.063	0.253

concentrations (ρ = 0.250, p = <0.001), GSH concentrations (ρ = 0.253, p = <0.001), GSSG concentrations (ρ = 0.123, p = 0.025), GSH/GSSG levels (ρ = 0.186, p = 0.001), and were negatively correlated with $NADP^+$/NADPH levels (ρ = −0.181, p = 0.001), and E_h levels (ρ = −0.307, p = <0.001).

Relationships between redox phenotypes and liver weights were also observed, with positive associations between liver weights and total glutathione concentrations (ρ = 0.137, p = 0.011), GSH concentrations (ρ = 0.136, p = 0.012), and GSSG concentrations (ρ = 0.176, p = 0.001). Liver weights were also positively correlated with NADPH concentrations (ρ = 0.203, p = <0.001) and negatively correlated with $NADP^+$ concentrations (ρ = −0.218, p = <0.001) and $NADP^+$/NADPH (ρ = −0.262, p = <0.001). NADH was not correlated with liver weight (ρ = −0.063, p = 0.253).

3.2. QTL mapping of the hepatic GSH redox system

We performed QTL analysis using R/qtl2 on all measured markers of the GSH redox system (Fig. 4). Here we outline the results of statistically significant peaks, yet it should be noted that multiple other peaks surpassed LOD scores of 6 but failed to surpass significance thresholds calculated through 1000 permutation tests. Genome-wide scans for hepatic concentrations of total glutathione and GSH revealed a suggestive peak (LOD scores 6.755 and 6.748, respectively) on mouse chromosome 14 (founder allele effects and candidate gene results are included in Supplementary Figures S2 and S3). Mapping GSH/GSSG and E_h revealed a significant (p-value ≤ 0.05) peak on mouse chromosome 16 at 8.998 Mbp (LOD scores 8.224 and 8.598, respectively). Given that the peak position was the same between the two scans, we focused on GSH/GSSG results, which are outlined in Fig. 5, while E_h results are provided in Supplementary Figure S4.

The genome-wide scan for GSH/GSSG revealed a significant peak on mouse chromosome 16 with a QTL interval of 8.865–10.077 Mbp (Fig. 5A). Within the interval, founder allele effects were extrapolated, showing that the AJ allele contributes to a higher GSH/GSSG, whereas the 129 allele contributes to a lower GSH/GSSG (Fig. 5B). Genes found within this interval ±1 Mbp were plotted using R/qtl2 through connection with the MGI database (Fig. 5C), and functional RNA and protein-coding genes were collected and screened for physiological relevance using existing expression, functional, and phenotypic annotations (Supplementary Table S7). The QTL interval contained 66 possible candidate genes: 29 protein-coding, 35 non-coding RNA, and 2 unclassified (GRCm38/mm10; gene query performed November 2020, Feature Type "gene" [78]). 30 of the 66 GSH/GSSG candidate genes had limited hepatic expression annotations and were therefore excluded. Of the remaining 36 candidate genes, 22 were limited to hepatic expression data only, and the remaining 14 candidate genes had annotations with functional relevance to the GSH redox system: transmembrane protein 114 (*Tmem114*), predicted gene 5767 (*Gm5767*), RIKEN cDNA 1810013L24 gene (*1810013L24Rik*), ribosomal protein L39-like (*Rpl39l*), activating transcription factor 7 interacting protein 2 (*Atf7ip2*), predicted gene 1600 (*Gm1600*), nucleotide binding protein 1 (*Nubp1*), *trans*-golgi network vesicle protein 23A (*Tvp23a*), class II transactivator (*Ciita*), *C*-type lectin domain family 16, member A (*Clec16a*), suppressor of cytokine signaling-1 (*Socs1*), protamine 3 (*Prm3*), protamine 2 (*Prm2*), and LPS-induced TN factor (*Litaf*). Based on functional and phenotypic annotations, *Socs1* (Chr16:10783808–10785536 bp; 5.81 cM; GRCm38) was determined to be the most likely candidate gene within the interval. SOCS1 functions as a negative regulator of cytokine signaling, including the JAK/STAT-signaling pathway, as well as insulin and toll-like receptor (TLR) signal transduction [84]. Importantly, SOCS1 has been involved in p53 activation and subsequent repression of the transcription of SLC7A11 [85] – a cystine/glutamate antiporter and regulator of intracellular cysteine concentrations, the rate-limiting precursor for GSH biosynthesis [86,87]. As a result of its suppression of *SLC7A11*, SOCS1 expression has been found to negatively correlate with GSH levels [85]. Furthermore, SOCS1 negatively regulates the nuclear factor-κB (NF-κB) transcription complex, specifically the p65 subunit, by acting as a ubiquitin ligase and prompting proteasome-mediated degradation [88]. NF-κB is transcription factor and activation of NF-κB is critical in maintaining cellular GSH concentrations [89] and expression of enzymes involved in GSH synthesis [90].

3.3. QTL mapping of the hepatic NAD(P)H phenotypes

Genome-wide scans were conducted for the following NADPH redox phenotypes: NADPH, $NADP^+$, $NADP^+$/NADPH, and NADH (Fig. 6). Scans for NADPH and NADH included peaks that surpassed LOD score 6 or more yet failed to reach significance. The genome-wide scan for $NADP^+$ revealed a suggestive peak (p-value≤0.20) on mouse chromosome 3 at 110.517 Mbp (LOD score 7.032) with a QTL interval of 109.677–115.729 Mbp (Fig. 7A). Founder allele effects showed that the WSB and PWK alleles contribute to a higher $NADP^+$ concentration, whereas the NOD and CAST alleles contribute to a lower $NADP^+$ concentration (Fig. 7B). Genes located within this interval ±1 Mbp were plotted using R/qtl2 (Fig. 7C) and existing biological annotations were

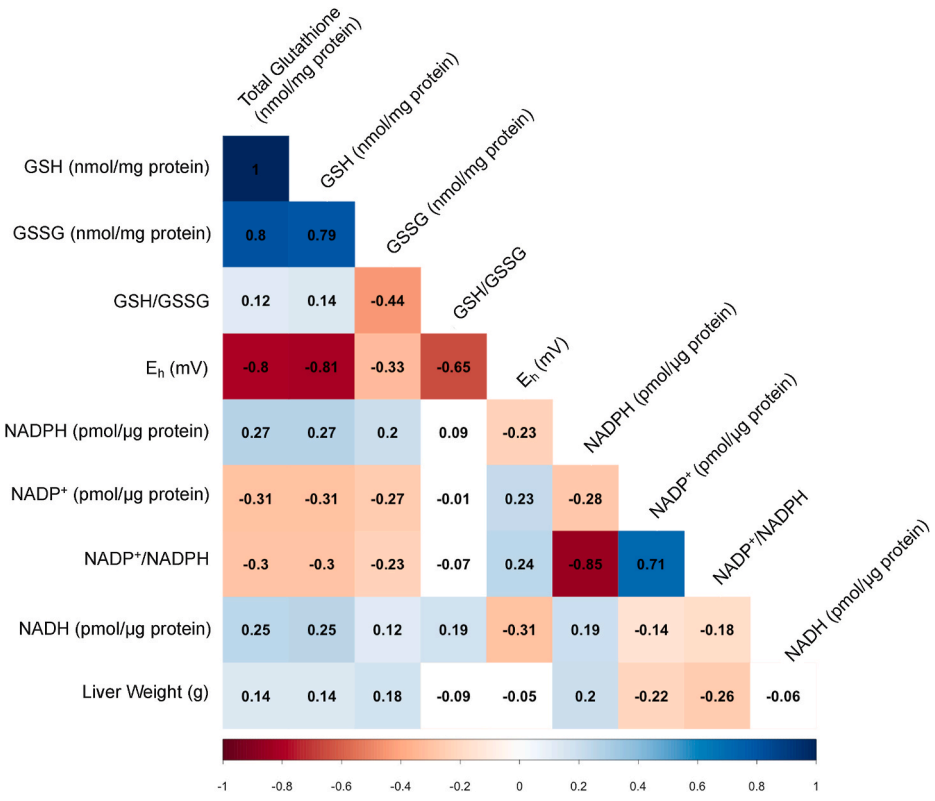

Fig. 3. Correlation matrix of statistical relationships among markers of the hepatic GSH redox system and liver weights. Spearman's rho (ρ) was calculated for each variable combination and is listed within each corresponding box. Total glutathione, GSH, and GSSG concentrations were standardized as nmol/mg protein. Concentrations of NADPH, NADP, and NADH were standardized as pmol/µg protein. E_h was expressed as mV. Liver weight was reported in grams (g). A colored box indicates a significant relationship ($p \leq 0.05$). An uncolored (white) box indicates an insignificant relationship ($p > 0.05$).

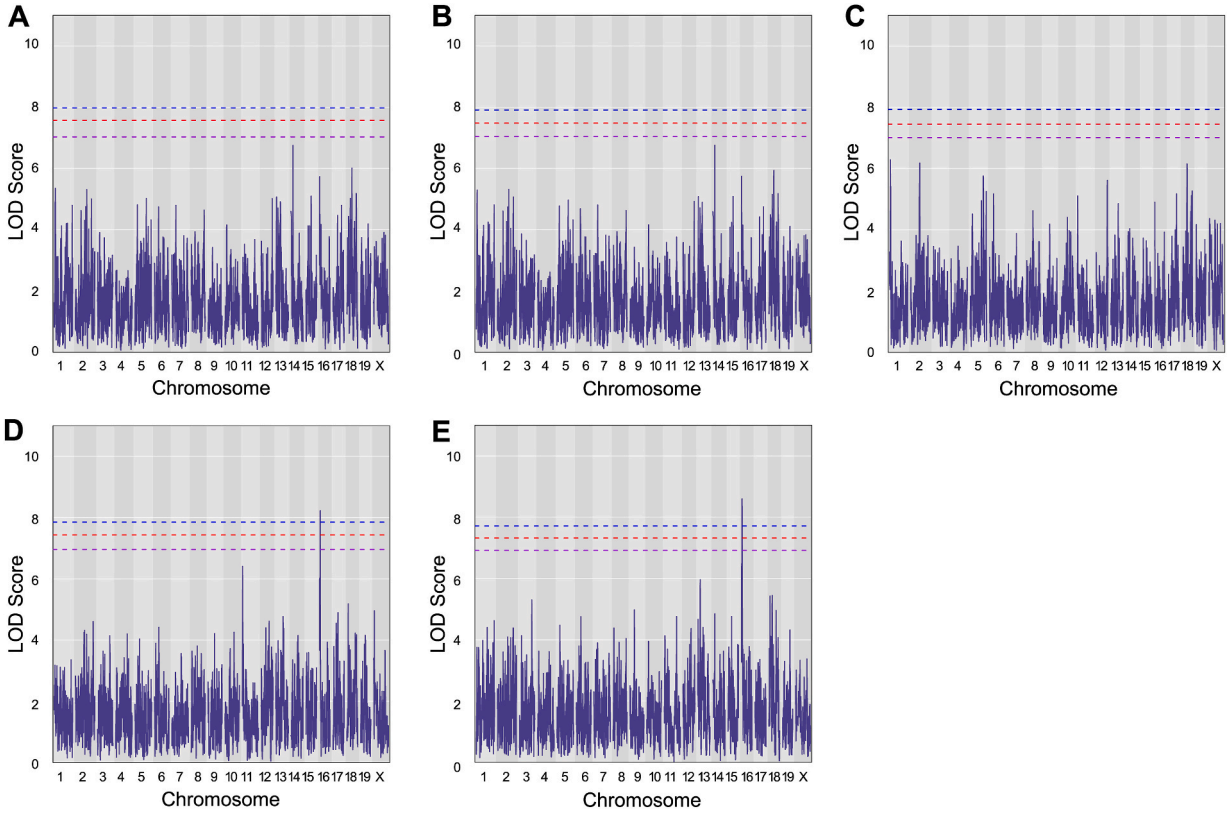

Fig. 4. QTL results for markers of the GSH redox system. Genome-wide scans of hepatic **A.** Total Glutathione (GSH+2GSSG, expressed in nmol/mg); **B.** GSH (nmol/mg); **C.** GSSG (nmol/mg); **D.** GSH/GSSG; and **E.** Redox Potential of the GSSG-GSH couple (E_h, expressed as mV). Permutation-derived significance thresholds are indicated by colored lines at significance (α) levels 0.05 (blue), 0.1 (red), and 0.2 (purple). (For interpretation of the references to color in this figure legend, the reader is referred to the Web version of this article.)

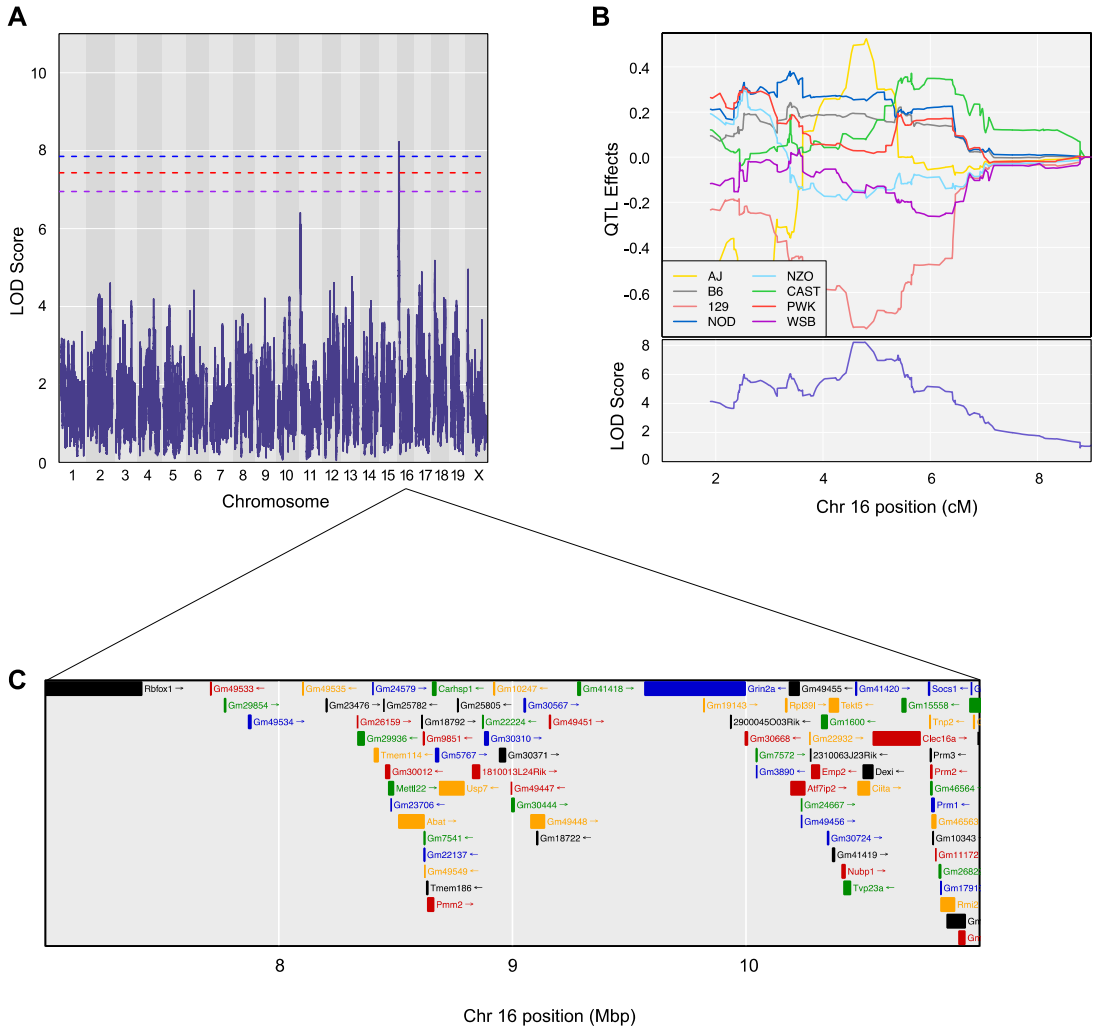

Fig. 5. High-resolution association mapping for hepatic GSH/GSSG in outbred mice reveals a significant QTL on mouse chromosome 16. **A.** Genome-wide scan of hepatic GSH/GSSG in outbred mice shows a QTL with peak LOD score 8.224 at 8.998 Mbp (4.779 cM) on mouse chromosome 16. Permutation-derived significance thresholds are indicated by colored lines at significance (α) levels 0.05 (blue), 0.1 (red), and 0.2 (purple). **B.** The founder allele QTL effects indicate that the 129 allele contributes to a lower hepatic GSH/GSSG concentration, whereas the AJ allele contributes to a higher hepatic GSH/GSSG concentration. Each colored line represents a DO founder allele as indicated in the legend. The differences between strains are considered significant when the LOD score (bottom) crosses significance thresholds (panel A). **C.** Candidate genes found within the QTL interval relative to the MGI database. E_h (mV) genome scan resulted in the same significant QTL interval on mouse chromosome 16 compared to GSH/GSSG (Supplementary Figure S4). (For interpretation of the references to color in this figure legend, the reader is referred to the Web version of this article.)

collected. The QTL interval contained 85 possible candidate genes: 38 protein-coding, 37 non-coding RNA, and 10 unclassified (Supplementary Table S8; GRCm38/mm10; gene query performed November 2020, Feature Type "gene" [78]). 52 of the 85 $NADP^+$ candidate genes had no hepatic expression and were therefore excluded. Of the remaining 33 candidate genes, 8 had no additional functional or phenotypic annotations related to hepatic redox function. The remaining 25 candidate genes were: chloride channel CLIC-like 1 (*Clcc1*), G-protein signaling modulator 2 (*Gpsm2*), AKNA domain containing 1 (*Aknad1*), syntaxin binding protein 3 (*Stxbp3*), PRP38 pre-mRNA processing factor 38 (yeast) domain containing B (*Prpf38b*), HEN1 methyltransferase homolog 1 (*Henmt1*), family with sequence similarity 102, member B (*Fam102b*), solute carrier family 25, member 54 (*Slc25a54*), vav 3 oncogene (*Vav3*), netrin G1 (*Ntng1*), protein arginine *N*-methyltransferase 6 (*Prmt6*), RNA-binding region containing 3 (*Rnpc3*), olfactomedin 3 (*Olfm3*), RIKEN cDNA A930005H10 gene (*A930005H10Rik*), diphthamide biosynthesis 5 (*Dph5*), solute carrier family 30 (zinc transporter), member 7 (*Slc30a7*), exostoses-like 2 (*Extl2*), vascular cell adhesion molecule 1 (*Vcam1*), CDC14 cell division cycle 14A (*Cdc14a*), RNA 3′-terminal phosphate cyclase (*Rtca*), dihydrolipoamide branched chain transacylase E2 (*Dbt*), leucine rich repeat containing 39 (*Lrrc39*), tRNA methyltransferase 13 (*Trmt13*), SAS-6 centriolar assembly protein (*Sass6*), and solute carrier family 35 (UDP-*N*-acetylglucosamine (UDP-GlcNAc) transporter), member 3 (*Slc35a3*). Evaluation of functional and phenotypic annotations did not point to a single candidate with a direct link to $NADP^+$ regulation. Yet a subsequent literature search suggested that *Vav3, Vcam1,* and *Cdc14a* were the most likely genes influencing $NADP^+$ concentrations. Vav3 (Chr3:109340653–109685698 bp; 48.13 cM; GRCm38) is a Rho GTPase regulating guanine nucleotide exchange factor (GEF) [91]. The Vav protein family, including Vav3, are key activators of the Card9/NF-κB pathway in immunity [92]. VCAM-1 (Chr3: 116110020–116129688 bp; 50.17 cM; GRCm38) expression is upregulated by NF-κB and increases in oxidative stress [93,94], and VCAM-1 activates NADPH oxidase in

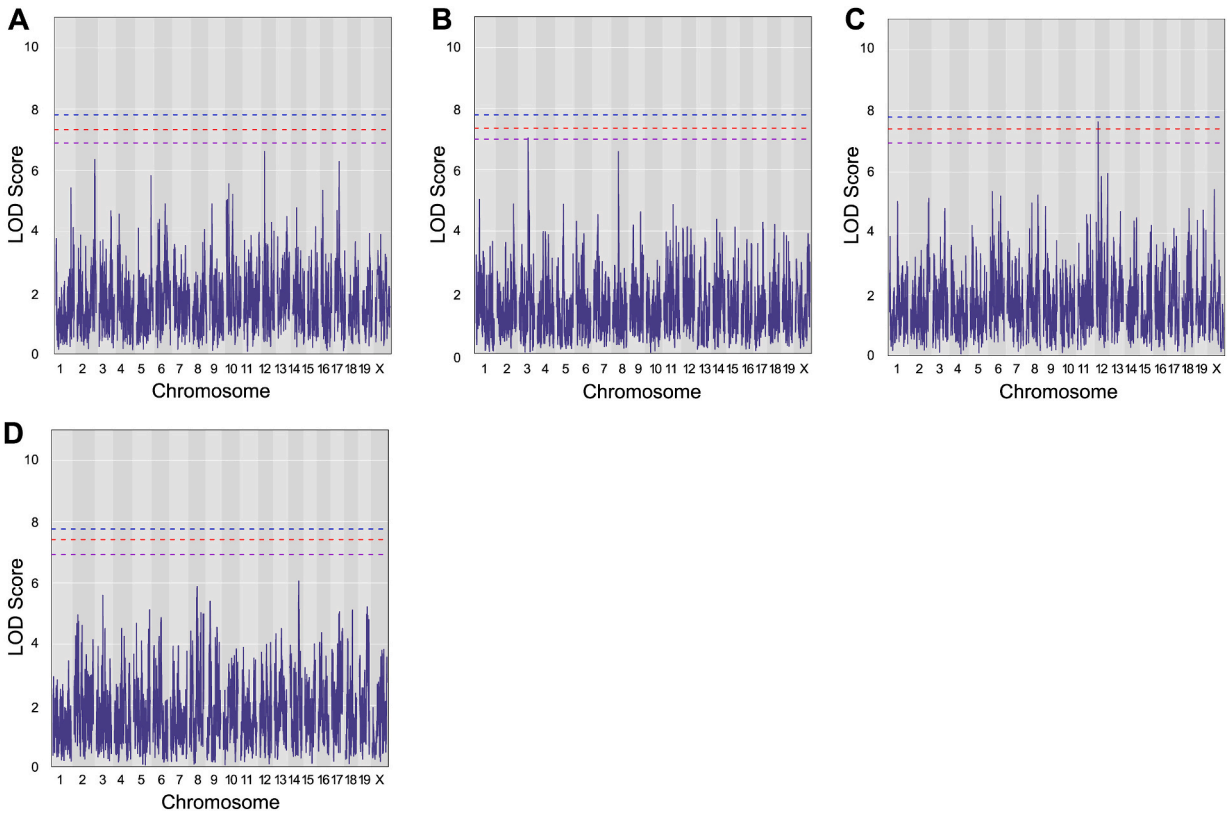

Fig. 6. QTL results for hepatic NAD(P)H phenotypes. Genome-wide scans of hepatic **A.** NADPH (pmol/μg); **B.** $NADP^+$ (pmol/μg); **C.** $NADP^+$/NADPH; and **D.** NADH (pmol/μg). Permutation-derived significance thresholds are indicated by colored lines at significance (α) levels 0.05 (blue), 0.1 (red), and 0.2 (purple). (For interpretation of the references to color in this figure legend, the reader is referred to the Web version of this article.)

endothelial cells [95]. CDC14A (Chr3: 116272553–116428741bp; 50.24 cM; GRCm38) is a phosphoprotein-phosphatase involved in cell cycle progression [96]. CDC14A has been found to dephosphorylate tumor suppressor p53 and is thought to regulate the function of p53 [97,98] whose actions are critical in regulating NADPH redox status and NADPH production through the pentose phosphate pathway [99,100]. We were unable to find research supporting the involvement of Vav3, Vcam-1, or Cdc14a's involvement with hepatic NF-κB or p53, nor their influence on hepatic $NADP^+$.

The genome-wide scan for $NADP^+$/NADPH revealed a suggestive peak (p-value≤0.10) on mouse chromosome 12 at 28.626 Mbp (LOD score 7.637) with a QTL interval of 28.562–29.394 Mbp (Fig. 8A). Founder allele effects were extrapolated within the interval and show that the WSB and B6 alleles contribute to a higher $NADP^+$/NADPH ratio, whereas the NOD and PWK alleles contribute to a lower $NADP^+$/NADPH ratio (Fig. 8B). Genes found within this credible interval ±1 Mbp were plotted using R/qtl2 through connection with the MGI database (Fig. 8C) for collection of functional RNA and protein coding genes. The QTL interval contained 51 possible candidate genes: 15 protein-coding, 34 non-coding RNA, and 2 unclassified (GRCm38/mm10; gene query performed November 2020, Feature Type "gene" [78]). Biological annotations were collected (Supplementary Table S9), and 36 of the 51 $NADP^+$/NADPH candidate genes had no hepatic expression annotations and were therefore excluded. 6 of the remaining 15 candidate genes did not have additional functional or phenotypic annotations related to hepatic redox function, and the remaining 9 candidate genes were: SRY (sex determining region Y)-box 11 (*Sox11*), collecting sub-family member 11 (*Colec11*), ribosomal protein S7 (*Rps7*), ribonuclease H1 (*Rnaseh1*), acireductone dioxygenase 1 (*Adi1*), myelin transcription factor 1-like (*Myt1l*), peroxidasin (*Pxdn*), thyroid peroxidase (*Tpo*), and syntrophin, gamma 2 (*Sntg2*). A comprehensive literature search on each gene failed to suggest evidence of their influence on hepatic $NADP^+$/NADPH levels or redox homeostasis.

4. Discussion

GSH is a core regulator of the cellular redox environment and its biochemistry has been thoroughly investigated since its discovery in the late 19th century [101]. Yet in recent years, studies have suggested that GSH is also controlled at a genetic level [48–53], though the specific loci and genes have remained unidentified. Here, we utilized the DO population, a model of human genetics, to map loci underlying indicators of the hepatic GSH redox system, including the essential cofactor NADPH and its precursor NADH. Through these efforts, we discovered novel loci and candidate genes responsible for hepatic GSH/GSSG, as well as $NADP^+$ and $NADP^+$/NADPH, shifting existing paradigms surrounding the role of genetics in redox regulation.

In this study, genome-wide association mapping revealed a novel locus for GSH/GSSG on murine chromosome 16 at 8.998 Mbp (p≤0.05), a region that contains 66 candidate genes. Via bioinformatic database query, we identified *Socs1* as the most plausible candidate gene for multiple reasons. First, *Socs1* is involved in the activation of p53 [85], a critical tumor suppressor that has been closely tied to redox systems and oxidative stress [102]. In low oxidative stress conditions, p53 augments antioxidant protection by upregulating *Gpx* and other stress resistance genes to ensure cell survival [102]. In high oxidative stress conditions, p53 acts as a prooxidant, increasing expression of prooxidative genes, such as proline oxidase, to initiate a stress cascade that ultimately leads to cell death [102]. In parallel to its upregulation of prooxidative genes, p53 inhibits nuclear factor E2-related factor 2 (Nrf2), a critical antioxidant transcription factor [103], ultimately repressing the expression of genes involved in glutathione metabolism (namely, *GCLM, GCLC, GR*, and cysteine transporter *SLC7A11*) [104–106]. SLC7A11, also referred to as *xCT*, is the regulator of intracellular cysteine, the essential

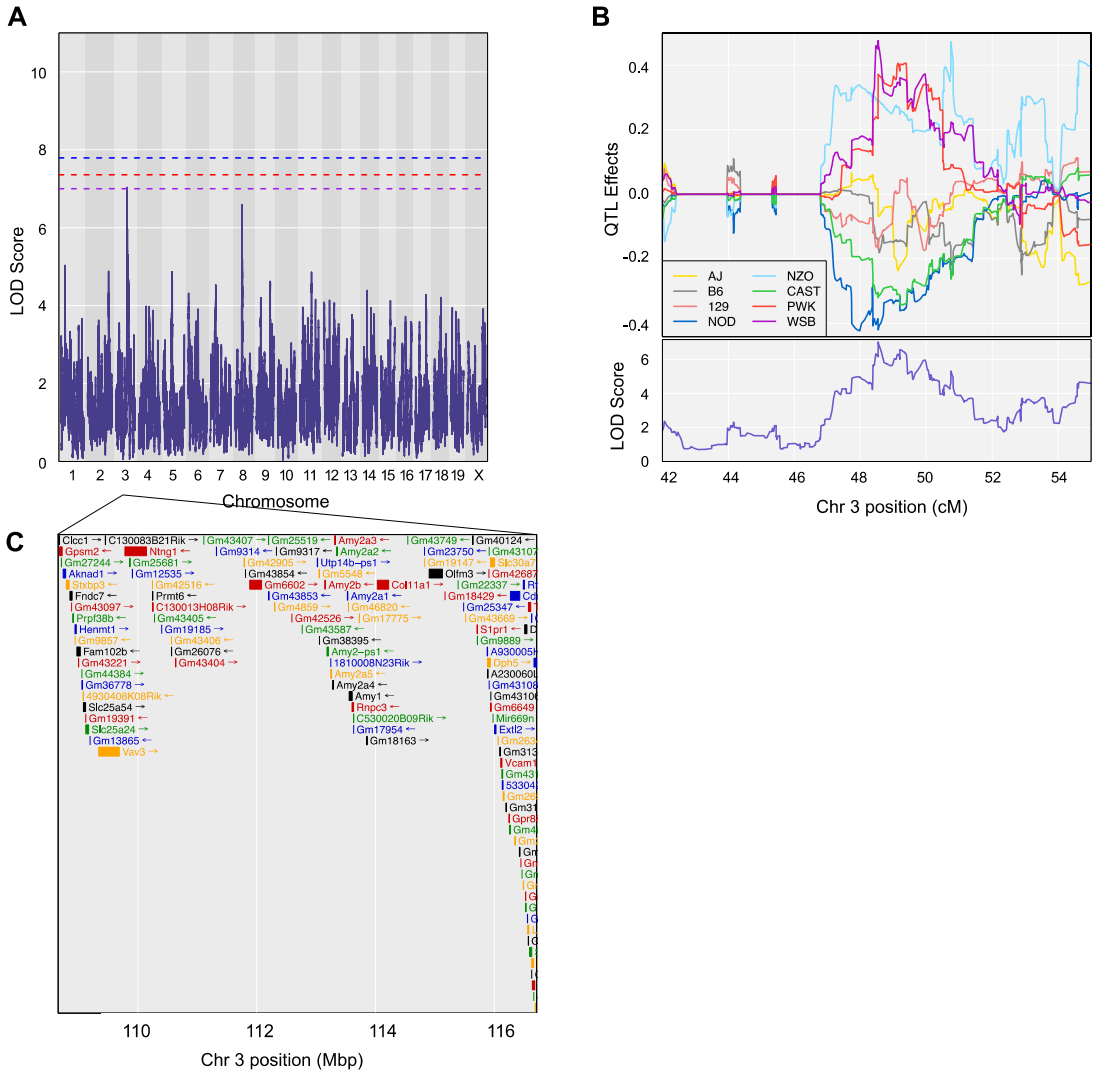

Fig. 7. High-resolution association mapping of hepatic $NADP^+$ reveals a suggestive QTL on mouse chromosome 3. **A.** Genome-wide scan of hepatic $NADP^+$ (pmol/μg) in outbred mice shows a QTL with peak LOD score 7.032 at 110.517 Mbp (48.547 cM) on mouse chromosome 3. Permutation-derived significance thresholds are indicated by colored lines at significance (α) levels 0.05 (blue), 0.1 (red), and 0.2 (purple). **B.** The founder allele QTL effects indicate that the NOD and CAST alleles contribute to a lower hepatic $NADP^+$ concentration, whereas the WSB and PWK alleles contribute to a higher hepatic $NADP^+$ concentration. Each colored line represents a DO founder allele as indicated in the legend. The differences between strains are considered significant when the LOD score (bottom) crosses significance thresholds (panel A). **C.** Candidate genes found within the QTL interval relative to the MGI database. (For interpretation of the references to color in this figure legend, the reader is referred to the Web version of this article.)

rate-limiting precursor to GSH biosynthesis [86,87,107,108]. Importantly, this full pathway has been validated, confirming that SOCS1 activates p53, driving declines in both *SLC7A11* expression and GSH levels [85]. Our results now suggest that variation in the *SOCS1* gene may have a similar effect.

In addition to its effect on p53 signaling, SOCS1 controls GSH levels via another prominent transcription factor: NF-κB [84]. NF-kB is responsive to oxidative stress, and upon activation, it controls expression of GCLC and GCLM, to increase GSH biosynthesis [89,90], and upregulates other antioxidant and anti-apoptotic proteins [109]. SOCS1 regulates the NF-κB complex by acting as a ubiquitin ligase, specifically at the p65 subunit, and prompting proteasome-mediated degradation [88,110–112]. Future research will investigate if promotion of NF-κB degradation by SOCS1 drives a decline in GSH biosynthesis.

To determine whether SOCS1 has been associated with liver function, we queried databases and published literature. In mice, *Socs1* expression was positively associated with hepatic necrosis (MP:0001654), hepatic steatosis (MP:0002628), liver degeneration (MP:0003103), and liver inflammation (MP:0001860) [78,113]. Yet interestingly, *Socs1*$^{-/-}$ knockout mice are rendered perinatal lethal [114], and gene deletion resulted in severe liver inflammation [114]. Furthermore, *Socs1* methylation in mouse liver is associated with advancement of liver fibrosis [114]. Therefore, both increases and decreases in *Socs1* expression have been associated with liver dysfunction in rodents. In humans, a *SOCS1* variant (rs243330) was associated with non-alcoholic fatty liver disease and insulin resistance in obese individuals [115]. Based on these findings, we propose that *Socs1* negatively regulates hepatic GSH via p53 and NF-kB, ultimately impeding liver function. Additional studies are needed to validate the specific effect of Socs1 on GSH/GSSG and better understand its impact on liver disease.

Next, we mapped phenotypes related to the cofactor NADPH and discovered suggestive QTL for $NADP^+$ on mouse chromosome 3 at 110.517 Mbp ($p \leq 0.20$) and $NADP^+$/NADPH on mouse chromosome 12 at 28.626 Mbp ($p \leq 0.10$). Candidate gene analysis for $NADP^+$ and $NADP^+$/NADPH was inconclusive, with a possible 25 candidate genes

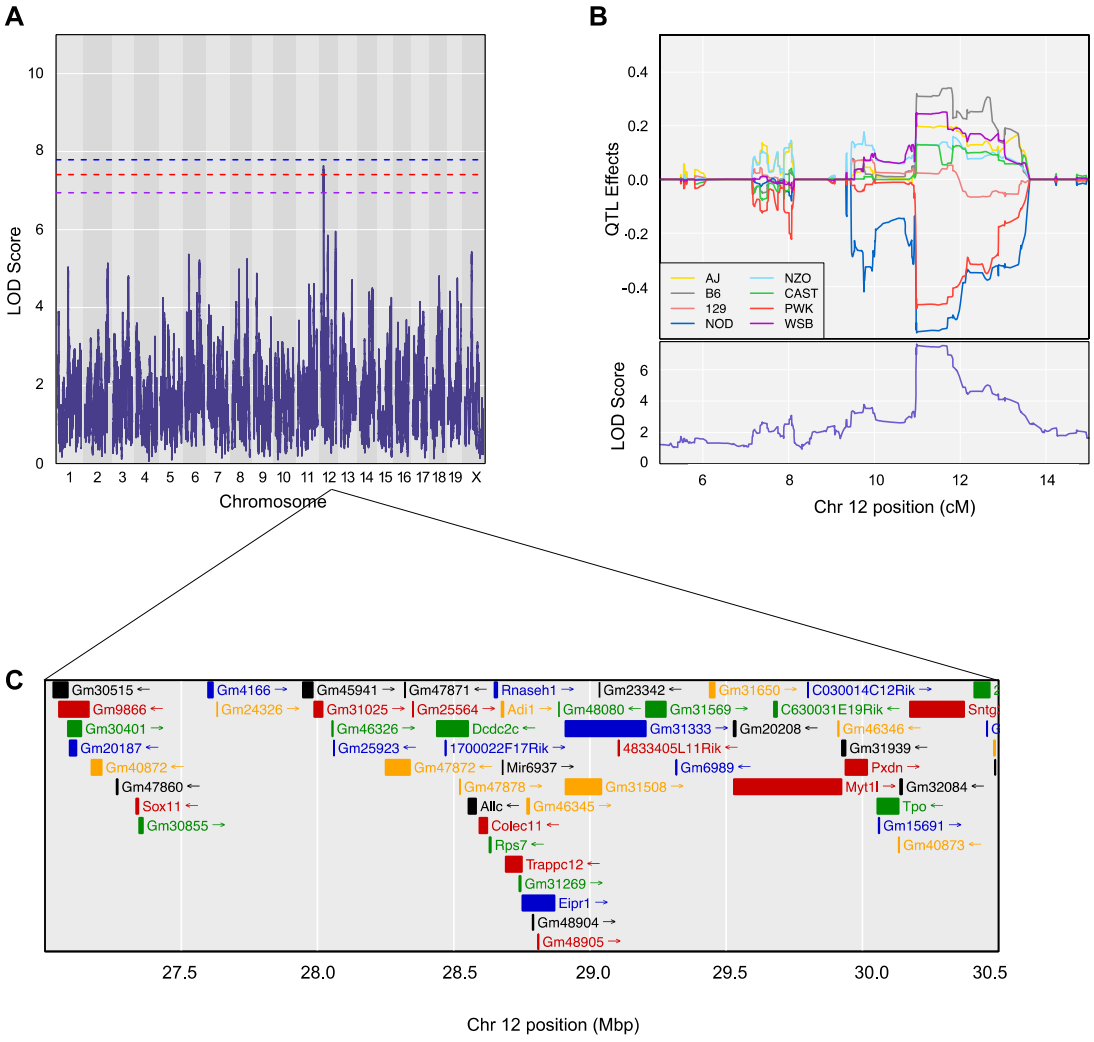

Fig. 8. High-resolution association mapping of hepatic NADP$^+$/NADPH reveals a suggestive QTL on mouse chromosome 12. **A.** Genome-wide scan of GSH in outbred mice shows a QTL with peak LOD score 7.637 at 28.626 Mbp (10.987 cM) on mouse chromosome 12. Permutation-derived significance thresholds are indicated by colored lines at significance (α) levels 0.05 (blue), 0.1 (red), and 0.2 (purple). **B.** The founder allele QTL effects indicate that the NOD and PWK alleles contribute to a lower hepatic NADP$^+$/NADPH concentration, whereas the WSB and B6 alleles contribute to a higher hepatic NADP$^+$/NADPH concentration. Each colored line represents a DO founder allele as indicated in the legend. The differences between strains are considered significant when the LOD score (bottom) crosses significance thresholds (panel A). **C.** Candidate genes found within the QTL interval relative to the MGI database. (For interpretation of the references to color in this figure legend, the reader is referred to the Web version of this article.)

for NADP$^+$ (*Clcc1, Gpsm2, Aknad1, Stxbp3, Prpf38b, Henmt1, Fam102b, Slc25a54, Vav3, Ntng1, Prmt6, Rnpc3, Olfm3, A930005H10Rik, Dph5, Slc30a7, Extl2, Vcam1, Cdc14a, Rtca, Dbt, Lrrc39, Trmt13, Sass6,* and *Slc35a3*) and 9 candidate genes for NADP$^+$/NADPH (*Sox11, Colec11, Rps7, Rnaseh1, Adi1, Myt1l, Pxdn, Tpo,* and *Sntg2*). A collection of functional and phenotypic annotations suggests that *Vav3, Vcam1,* and *Cdc14a* are the most likely genes influencing NADP$^+$ concentrations, though they have no documented roles in hepatic redox metabolism. Future studies will be conducted to narrow and eventually select the causative gene.

Previous genetics research used *in silico* haplotype association mapping (HAM) to identify novel loci associated with hepatic and renal GSH and GSSG concentrations, as well as GSH/GSSG [51]. We compared those loci to all QTL peaks with LOD scores >6 from the present study (Supplementary Table S10) to find any loci overlapping between studies. We did not observe any direct overlap between the previous HAM results and the current QTL study. Yet we found alignment between our QTL peak for NADP$^+$ on mouse chromosome 8 at 61.237 (60.722–65.378) Mbp and HAM peaks for hepatic GSH on mouse chromosome 8 at 56.109 Mbp and renal GSSG on mouse chromosome 8 at 54.793 and 55.416 Mbp. Moreover, we documented a QTL peak for hepatic GSSG on chromosome 1 at 21.043 (18.793–22.050) Mbp which was near the HAM peak observed for renal GSH on chromosome 1 at 20.259 Mbp. Overall, these results indicate that there could be shared regulatory mechanisms between the hepatic and renal GSH redox systems, and new research will need to investigate these relationships further.

Notable in this study was the absence of loci overlapping with canonical genes involved in GSH synthesis and metabolism. We posited that no such loci were found because DO mice lack significant variation in those genes. Using R/qtl2, we visualized founder allele effects in the genetic regions of *Gpx1*, *Gclc*, *Gclm*, *Gs*, and *Gr* (Supplementary Table S11) [113] and concluded that those gene locations contained no variation that would significantly increase or decrease the phenotype (Supplementary Figure S5 – S9). Our results support previous conclusions that variation in hepatic GSH is not driven by canonical genes responsible for GSH synthesis and recycling [51], but rather by novel regulatory loci in mouse models.

The DO stock is a model of human genetic variation [116] with over 39.8 million documented single nucleotide polymorphisms (SNPs) available for genome-wide association studies (GWAS), compared to the human 1000 Genomes Project which had only 8.1 million SNPs available for GWAS [D. Gatti, personal communication, May 5, 2021]. Furthermore, the DO population exhibits traits similar to those of human disease [69] and may be useful for modeling human variation in phenotypes that are not readily measurable in patients. For instance, GSH status [5,117] and circulating GSH/GSSG [118] have been tied to liver disease severity, yet it is unclear how hepatic GSH varies in the broader human population. Here, in the DO stock, we observed substantial variation in GSH phenotypes, with an 11-fold difference in total glutathione and GSH concentrations, a 16-fold difference in GSSG concentrations, and over a 5-fold difference in GSH/GSSG. Moreover, liver weight, which has been tied to NAFLD [119], exhibited an approximately 5.5-fold variation and correlated with hepatic GSH and GSSG. Based on our knowledge of this model and its relevance to the human condition, we predict that human populations may see similar differences in hepatic GSH among individuals, though such a hypothesis must be carefully addressed in future studies.

It must be noted that the present study was accompanied by some limitations. Though male and female mice were used in near-equal numbers, a subset of males (N = 63) had to be individually housed due to aggressive behavior. Excessive fighting has been associated with additive stress in mice [120], which had the potential of negatively influencing GSH due to the molecule's sensitivity toward external stressors [52]. To address this issue, we performed Mann-Whitney tests comparing variables in mice to their housing group size and found that singly-housed mice did not have significantly different levels of GSH, NAD(P)H, their redox balances, or liver weights compared to those housed in greater numbers. Furthermore, to avoid the possibility of oxidation from prolonged exposure on the HPLC sample plate, all samples were thawed on the sample plate at 4°C and analyzed in duplicates within 4 h of being put on the plate.

5. Conclusion

Here, for the first time, the GSH redox system was explored using an innovative, powerful systems genetics approach. We discovered a novel locus associated with hepatic GSH/GSSG on murine chromosome 16 and identified *Socs1* as the most likely candidate gene within the region, a decision informed by the gene's established roles in redox homeostasis and inflammation. Future mechanistic studies will continue investigations into *Socs1* as a central genetic regulator of GSH homeostasis, and the results will considerably expand our understanding of GSH and the mechanisms that control it. Subsequent studies will also probe the newly discovered loci associated with NAD(P)H dynamics. As genome-wide association studies in mice are crucial for isolating and identifying candidate genes to test in human trials, we expect that *SOCS1* and other candidates will be interrogated in future clinical studies as well. Overall, these results establish a framework for studying redox biochemical pathways using systems genetics tools such as the DO.

Funding sources

This work was supported by the following National Institutes of Health grants: National Institute of General Medical Sciences R01 GM121551 and the National Institute on Aging R56 AG053309.

Declaration of competing interest

The authors declare that there are no conflicts of interest.

Acknowledgements

The authors gratefully acknowledge Greg Keele, Vivek Phillip, Belinda Cornes, and Dan Gatti for their assistance with the genetic mapping process, Kim Love for her help with statistical calculations, Kristen Peissig, Mallory Johns, Kylah Chase, Aida Rassam, Tina Heydari, Lynsey Young, and Madeleine Williams for their assistance with the data collection, and Ali Ennis for creating the graphical abstract.

Appendix A. Supplementary data

Supplementary data to this article can be found online at https://doi.org/10.1016/j.redox.2021.102093.

References

[1] J. Pizzorno, Glutathione!, Integr. Med. 13 (1) (2014) 8–12.
[2] J.R. Grunwell, S.E. Gillespie, J.M. Ward, A.M. Fitzpatrick, L.A. Brown, T. W. Gauthier, K.B. Hebbar, Comparison of glutathione, cysteine, and their redox potentials in the plasma of critically ill and healthy children, Front Ped 3 (2015) 46, 46.
[3] C. Berndt, C.H. Lillig, A. Holmgren, Thioredoxins and glutaredoxins as facilitators of protein folding, Biochim. Biophys. Acta Mol. Cell Res. 1783 (4) (2008) 641–650.
[4] E. Kalinina, M. Novichkova, Glutathione in protein redox modulation through S-glutathionylation and S-nitrosylation, Molecules 26 (2) (2021).
[5] S.C. Lu, Dysregulation of glutathione synthesis in liver disease, Liver Res 4 (2) (2020) 64–73.
[6] C. Loguercio, D. Taranto, L.M. Vitale, F. Beneduce, C. Del Vecchio Blanco, Effect of liver cirrhosis and age on the glutathione concentration in the plasma, erythrocytes, and gastric mucosa of man, Free Radic. Biol. Med. 20 (3) (1996) 483–488.
[7] F. Santangelo, V. Witko-Sarsat, T. Drüeke, B. Descamps-Latscha, Restoring glutathione as a therapeutic strategy in chronic kidney disease, Nephrol. Dial. Transplant. 19 (8) (2004) 1951–1955.
[8] X.C. Ling, K.-L. Kuo, Oxidative stress in chronic kidney disease, Ren Replace Ther 4 (1) (2018) 53.
[9] H. Shimizu, Y. Kiyohara, I. Kato, T. Kitazono, Y. Tanizaki, M. Kubo, H. Ueno, S. Ibayashi, M. Fujishima, M. Iida, Relationship between plasma glutathione levels and cardiovascular disease in a defined population: the Hisayama study, Stroke 35 (9) (2004) 2072–2077.
[10] T. Damy, M. Kirsch, L. Khouzami, P. Caramelle, P. Le Corvoisier, F. Roudot-Thoraval, J.-L. Dubois-Randé, L. Hittinger, C. Pavoine, F. Pecker, Glutathione deficiency in cardiac patients is related to the functional status and structural cardiac abnormalities, PloS One 4 (3) (2009) e4871, e4871.
[11] K. Gawlik, J.W. Naskalski, D. Fedak, D. Pawlica-Gosiewska, U. Grudzień, P. Dumnicka, M.T. Małecki, B. Solnica, Markers of antioxidant defense in patients with type 2 diabetes, Oxid Med Cell Longev (2016) 2352361.
[12] I. Hakki Kalkan, M. Suher, The relationship between the level of glutathione, impairment of glucose metabolism and complications of diabetes mellitus, Pak J Biol Sci 29 (4) (2013) 938–942.
[13] V. Calabrese, C. Cornelius, V. Leso, A. Trovato-Salinaro, B. Ventimiglia, M. Cavallaro, M. Scuto, S. Rizza, L. Zanoli, S. Neri, P. Castellino, Oxidative stress, glutathione status, sirtuin and cellular stress response in type 2 diabetes, Biochim. Biophys. Acta 1822 (5) (2012) 729–736.
[14] M.J. Picklo, E.K. Long, E.E. Vomhof-DeKrey, Glutathionyl systems and metabolic dysfunction in obesity, Nutr. Rev. 73 (12) (2015) 858–868.
[15] C. Méplan, L.O. Dragsted, G. Ravn-Haren, A. Tjønneland, U. Vogel, J. Hesketh, Association between polymorphisms in glutathione peroxidase and selenoprotein P genes, glutathione peroxidase activity, HRT use and breast cancer risk, PloS One 8 (9) (2013), e73316.
[16] M. Udler, A.T. Maia, A. Cebrian, C. Brown, D. Greenberg, M. Shah, C. Caldas, A. Dunning, D. Easton, B. Ponder, P. Pharoah, Common germline genetic variation in antioxidant defense genes and survival after diagnosis of breast cancer, J. Clin. Oncol. 25 (21) (2007) 3015–3023.
[17] Z. Corredor, M.I.d.S. Filho, L. Rodríguez-Ribera, A. Velázquez, A. Hernández, C. Catalano, K. Hemminki, E. Coll, I. Silva, J.M. Diaz, J. Ballarin, M. Vallés Prats, J. Calabia Martínez, A. Försti, R. Marcos, S. Pastor, Genetic variants associated with chronic kidney disease in a Spanish population, Sci. Rep. 10 (1) (2020) 144.
[18] Z. Arsova-Sarafinovska, N. Matevska, A. Eken, D. Petrovski, S. Banev, S. Dzikova, V. Georgiev, A. Sikole, O. Erdem, A. Sayal, A. Aydin, A.J. Dimovski, Glutathione peroxidase 1 (GPX1) genetic polymorphism, erythrocyte GPX activity, and prostate cancer risk, Int. Urol. Nephrol. 41 (1) (2009) 63–70.
[19] C. Bănescu, M. Iancu, A.P. Trifa, M. Cândea, E. Benedek Lazar, V.G. Moldovan, C. Duicu, F. Tripon, A. Crauciuc, M. Dobreanu, From six gene polymorphisms of the antioxidant system, only GPX Pro198Leu and GSTP1 Ile105Val modulate the risk of acute myeloid leukemia, Oxid Med Cell Longev (2016) 2536705.
[20] K. Mohammedi, T.A. Patente, N. Bellili-Muñoz, F. Driss, H. Le Nagard, F. Fumeron, R. Roussel, S. Hadjadj, M.L. Corrêa-Giannella, M. Marre, G. Velho, Glutathione peroxidase-1 gene (GPX1) variants, oxidative stress and risk of

kidney complications in people with type 1 diabetes, Metabolism 65 (2) (2016) 12–19.
[21] B. Voetsch, R.C. Jin, C. Bierl, K.S. Benke, G. Kenet, P. Simioni, F. Ottaviano, B. P. Damasceno, J.M. Annichino-Bizacchi, D.E. Handy, J. Loscalzo, Promoter polymorphisms in the plasma glutathione peroxidase (GPx-3) gene: a novel risk factor for arterial ischemic stroke among young adults and children, Stroke 38 (1) (2007) 41–49.
[22] A.I. Rupérez, J. Olza, M. Gil-Campos, R. Leis, M.D. Mesa, R. Tojo, R. Cañete, A. Gil, C.M. Aguilera, Association of genetic polymorphisms for glutathione peroxidase genes with obesity in Spanish children, Lifestyle Genom 7 (3) (2014) 130–142.
[23] J. Ahn, M.D. Gammon, R.M. Santella, M.M. Gaudet, J.A. Britton, S.L. Teitelbaum, M.B. Terry, A.I. Neugut, C.B. Ambrosone, No association between glutathione peroxidase Pro198Leu polymorphism and breast cancer risk, Cancer Epidemiol. Biomarkers Prev. 14 (10) (2005) 2459–2461.
[24] A. Aydin, Z. Arsova-Sarafinovska, A. Sayal, A. Eken, O. Erdem, K. Erten, Y. Ozgök, A. Dimovski, Oxidative stress and antioxidant status in non-metastatic prostate cancer and benign prostatic hyperplasia, Clin. Biochem. 39 (2) (2006) 176–179.
[25] H. Dursun, M. Bilici, A. Uyanik, N. Okcu, M. Akyüz, Antioxidant enzyme activities and lipid peroxidation levels in erythrocytes of patients with oesophageal and gastric cancer, J. Int. Med. Res. 34 (2) (2006) 193–199.
[26] Z. Pawłowicz, B.A. Zachara, U. Trafikowska, A. Maciag, E. Marchaluk, A. Nowicki, Blood selenium concentrations and glutathione peroxidase activities in patients with breast cancer and with advanced gastrointestinal cancer, J. Trace Elem. Electrolytes Health & Dis. 5 (4) (1991) 275–277.
[27] G. Ravn-Haren, A. Olsen, A. Tjønneland, L.O. Dragsted, B.A. Nexø, H. Wallin, K. Overvad, O. Raaschou-Nielsen, U. Vogel, Associations between GPX1 Pro198Leu polymorphism, erythrocyte GPX activity, alcohol consumption and breast cancer risk in a prospective cohort study, Carcinogenesis 27 (4) (2006) 820–825.
[28] E.I. Saygili, T. Akcay, D. Konukoglu, C. Papilla, Glutathione and glutathione-related enzymes in colorectal cancer patients, J. Toxicol. Environ. Health 66 (5) (2003) 411–415.
[29] E. Ristoff, A. Larsson, Patients with genetic defects in the gamma-glutamyl cycle, Chem. Biol. Interact. 111–112 (1998) 113–121.
[30] E.F. McKone, J. Shao, D.D. Frangolias, C.L. Keener, C.A. Shephard, F.M. Farin, M. R. Tonelli, P.D. Pare, A.J. Sandford, M.L. Aitken, T.J. Kavanagh, Variants in the glutamate-cysteine-ligase gene are associated with cystic fibrosis lung disease, Am. J. Respir. Crit. Care Med. 174 (4) (2006) 415–419.
[31] A.R. Bentley, P. Emrani, P.A. Cassano, Genetic variation and gene expression in antioxidant related enzymes and risk of COPD: a systematic review, Thorax 63 (11) (2008) 956–961.
[32] A. Yuniastuti, R. Susanti, D. Mustikaningtyas, Polymorphism of glutamate-cysteine ligase subunit catalytic (GCLC) gene in pulmonary tuberculosis patients, Pak J Biol Sci 20 (8) (2017) 397–402.
[33] A.C. Walsh, J.A. Feulner, A. Reilly, Evidence for functionally significant polymorphism of human glutamate cysteine ligase catalytic subunit: association with glutathione levels and drug resistance in the national cancer Institute tumor cell line panel, Toxicol. Sci. 61 (2) (2001) 218–223.
[34] H.M. Custodio, K. Broberg, M. Wennberg, J.H. Jansson, B. Vessby, G. Hallmans, B. Stegmayr, S. Skerfving, Polymorphisms in glutathione-related genes affect methylmercury retention, Arch. Environ. Health 59 (11) (2004) 588–595.
[35] S. Koide, K. Kugiyama, S. Sugiyama, S. Nakamura, H. Fukushima, O. Honda, M. Yoshimura, H. Ogawa, Association of polymorphism in glutamate-cysteine ligase catalytic subunit gene with coronary vasomotor dysfunction and myocardial infarction, J. Am. Coll. Cardiol. 41 (4) (2003) 539–545.
[36] L. Skvortsova, A. Perfelyeva, E. Khussainova, A. Mansharipova, H.J. Forman, L. Djansugurova, Association of GCLM -588C/T and GCLC -129T/C promoter polymorphisms of genes coding the subunits of glutamate cysteine ligase with ischemic heart disease development in Kazakhstan population, Dis. Markers (2017) 4209257.
[37] S.-i. Nakamura, S. Sugiyama, D. Fujioka, K.-i. Kawabata, H. Ogawa, K. Kugiyama, Polymorphism in glutamate-cysteine ligase modifier subunit gene is associated with impairment of nitric oxide–mediated coronary vasomotor function, Circulation 108 (12) (2003) 1425–1427.
[38] M. Tosic, J. Ott, S. Barral, P. Bovet, P. Deppen, F. Gheorghita, M.L. Matthey, J. Parnas, M. Preisig, M. Saraga, A. Solida, S. Timm, A.G. Wang, T. Werge, M. Cuénod, K.Q. Do, Schizophrenia and oxidative stress: glutamate cysteine ligase modifier as a susceptibility gene, Am. J. Hum. Genet. 79 (3) (2006) 586–592.
[39] T. Kishi, M. Ikeda, T. Kitajima, Y. Yamanouchi, Y. Kinoshita, K. Kawashima, T. Inada, M. Harano, T. Komiyama, T. Hori, M. Yamada, M. Iyo, I. Sora, Y. Sekine, N. Ozaki, H. Ujike, N. Iwata, Glutamate cysteine ligase modifier (GCLM) subunit gene is not associated with methamphetamine-use disorder or schizophrenia in the Japanese population, Ann. N. Y. Acad. Sci. 1139 (2008) 63–69.
[40] R. Hanzawa, T. Ohnuma, Y. Nagai, N. Shibata, H. Maeshima, H. Baba, T. Hatano, Y. Takebayashi, Y. Hotta, M. Kitazawa, H. Arai, No association between glutathione-synthesis-related genes and Japanese schizophrenia, Psychiatr. Clin. Neurosci. 65 (1) (2011) 39–46.
[41] Z. Sun, J. Chen, J. Aakre, R.S. Marks, Y.Y. Garces, R. Jiang, O. Idowu, J. M. Cunningham, Y. Liu, V.S. Pankratz, P. Yang, Genetic variation in glutathione metabolism and DNA repair genes predicts survival of small-cell lung cancer patients, Ann. Oncol. 21 (10) (2010) 2011–2016.
[42] C.V. Breton, M.T. Salam, H. Vora, W.J. Gauderman, F.D. Gilliland, Genetic variation in the glutathione synthesis pathway, air pollution, and children's lung function growth, Am. J. Respir. Crit. Care Med. 183 (2) (2011) 243–248.
[43] N. Dahl, M. Pigg, E. Ristoff, R. Gali, B. Carlsson, B. Mannervik, A. Larsson, P. Board, Missense mutations in the human glutathione synthetase gene result in severe metabolic acidosis, 5-oxoprolinuria, hemolytic anemia and neurological dysfunction, Hum. Mol. Genet. 6 (7) (1997) 1147–1152.
[44] K.M. Goebel, L. Hausmann, H. Kaffarnik, Pancytopenia with hemolytic anemia in glutathione reductase deficiency, Enzyme 12 (1971) 375–381.
[45] N.M. Kamerbeek, R. van Zwieten, M. de Boer, G. Morren, H. Vuil, N. Bannink, C. Lincke, K.M. Dolman, K. Becker, R.H. Schirmer, S. Gromer, D. Roos, Molecular basis of glutathione reductase deficiency in human blood cells, Blood 109 (8) (2007) 3560–3566.
[46] E. Beutler, T. Gelbart, T. Kondo, A.T. Matsunaga, The molecular basis of a case of gamma-glutamylcysteine synthetase deficiency, Blood 94 (8) (1999) 2890–2894.
[47] E. Ristoff, A. Larsson, Inborn errors in the metabolism of glutathione, Orphanet J. Rare Dis. 2 (2007) 16, 16.
[48] I. Rebrin, M.J. Forster, R.S. Sohal, Effects of age and caloric intake on glutathione redox state in different brain regions of C57BL/6 and DBA/2 mice, Brain Res. 1127 (1) (2007) 10–18.
[49] I. Rebrin, M.J. Forster, R.S. Sohal, Association between life-span extension by caloric restriction and thiol redox state in two different strains of mice, Free Radic. Biol. Med. 51 (1) (2011) 225–233.
[50] M. Ferguson, I. Rebrin, M.J. Forster, R. Sohal, Comparison of metabolic rate and oxidative stress between two different strains of mice with varying response to caloric restriction, Exp. Gerontol. 43 (8) (2008) 757–763.
[51] Y. Zhou, D.E. Harrison, K. Love-Myers, Y. Chen, A. Grider, K. Wickwire, J. R. Burgess, M.A. Stochelski, R. Pazdro, Genetic analysis of tissue glutathione concentrations and redox balance, Free Radic. Biol. Med. 71 (2014) 157–164.
[52] R.L. Gould, Y. Zhou, C.L. Yakaitis, K. Love, J. Reeves, W. Kong, E. Coe, Y. Xiao, R. Pazdro, Heritability of the aged glutathione phenotype is dependent on tissue of origin, Mamm. Genome 29 (9) (2018) 619–631.
[53] T.J. van 't Erve, B.A. Wagner, K.K. Ryckman, T.J. Raife, G.R. Buettner, The concentration of glutathione in human erythrocytes is a heritable trait, Free Radic. Biol. Med. 65 (2013) 742–749.
[54] E.J. Chesler, S.L. Rodriguez-Zas, J.S. Mogil, In silico mapping of mouse quantitative trait loci, Science 294 (5551) (2001) 2423.
[55] J.D. Smith, D. James, H.M. Dansky, K.M. Wittkowski, K.J. Moore, J.L. Breslow, Silico quantitative trait locus map for atherosclerosis susceptibility in apolipoprotein E–deficient mice, Arterioscler. Thromb. Vasc. Biol. 23 (1) (2003) 117–122.
[56] S.L. Burgess-Herbert, S.-W. Tsaih, I.M. Stylianou, K. Walsh, A.J. Cox, B. Paigen, An experimental assessment of in silico haplotype association mapping in laboratory mice, BMC Genet. 10 (1) (2009) 81.
[57] G.A. Churchill, D.M. Gatti, S.C. Munger, K.L. Svenson, The Diversity Outbred mouse population, Mamm. Genome 23 (9–10) (2012) 713–718.
[58] K.W. Broman, D.M. Gatti, P. Simecek, N.A. Furlotte, P. Prins, S. Sen, B.S. Yandell, G.A. Churchill, R/qtl2: software for mapping quantitative trait loci with high dimensional data and multi-parent populations, Genetics 211 (2) (2019) 495.
[59] R. Franco, O.J. Schoneveld, A. Pappa, M.I. Panayiotidis, The central role of glutathione in the pathophysiology of human diseases, Arch. Physiol. Biochem. 113 (4–5) (2007) 234–258.
[60] D.P. Jones, H. Sies, The redox code, Antioxid Redox Signal 23 (9) (2015) 734–746.
[61] H.J. Park, E. Mah, B. RS, Validation of high-performance liquid chromatography boron-doped diamond detection for assessing hepatic glutathione redox status, Anal. Biochem. 407 (2010) 151–159.
[62] K. Khazim, D. Giustarini, R. Rossi, D. Verkaik, J.E. Cornell, S.E.D. Cunningham, M. Mohammad, K. Trochta, C. Lorenzo, F. Folli, S. Bansal, P. Fanti, Glutathione redox potential is low and glutathionylated and cysteinylated hemoglobin levels are elevated in maintenance hemodialysis patients, Transl. Res. 162 (1) (2013) 16–25.
[63] X. Wang, Q. Wang, R. Andersson, S. Bengmark, Intramucosal pH and oxygen extraction in the gastrointestinal tract after major liver resection in rats, Eur. J. Surg. 159 (2) (1993) 81–87.
[64] T.R. Ziegler, A. Panoskaltsus-Mortari, L.H. Gu, C.R. Jonas, C.L. Farrell, D.L. Lacey, D.P. Jones, B.R. Blazar, Regulation of glutathione redox status in lung and liver by conditioning regimens and keratinocyte frowth factor in murine allogeneic bone marrow transplantation, Transplantation 72 (8) (2001).
[65] J. Rost, S. Rapoport, Reduction potential of glutathione, Nature 201 (1964) 185.
[66] I. Rebrin, S. Kamzalov, R.S. Sohal, Effects of age and caloric restriction on glutathione redox state in mice, Free Radic. Biol. Med. 35 (6) (2003) 626–635.
[67] J. García-de-la-Asunción, E. García-Del-Olmo, G. Galan, R. Guijarro, F. Martí, R. Badenes, J. Perez-Griera, A. Duca, C. Delgado, J. Carbonell, J. Belda, Glutathione oxidation correlates with one-lung ventilation time and PO2/FiO2 ratio during pulmonary lobectomy, Redox Rep. 21 (5) (2016) 219–226.
[68] A.P. Morgan, C.-P. Fu, C.-Y. Kao, C.E. Welsh, J.P. Didion, L. Yadgary, L. Hyacinth, M.T. Ferris, T.A. Bell, D.R. Miller, P. Giusti-Rodriguez, R.J. Nonneman, K.D. Cook, J.K. Whitmire, L.E. Gralinski, M. Keller, A.D. Attie, G.A. Churchill, P. Petkov, P. F. Sullivan, J.R. Brennan, L. McMillan, F. Pardo-Manuel de Villena, The mouse universal genotyping array: from substrains to subspecies, G3 6 (2) (2016) 263.
[69] K.L. Svenson, D.M. Gatti, W. Valdar, C.E. Welsh, R. Cheng, E.J. Chesler, A. A. Palmer, L. McMillan, G.A. Churchill, High-resolution genetic mapping using the mouse diversity outbred population, Genetics 190 (2) (2012) 437.
[70] J. Yang, N.A. Zaitlen, M.E. Goddard, P.M. Visscher, A.L. Price, Advantages and pitfalls in the application of mixed-model association methods, Nat. Genet. 46 (2) (2014) 100–106.
[71] S. Sen, G.A. Churchill, A statistical framework for quantitative trait mapping, Genetics 159 (1) (2001) 371–387.

[72] G.A. Churchill, R.W. Doerge, Empirical threshold values for quantitative trait mapping, Genetics 138 (3) (1994) 963–971.

[73] G.K. Robinson, That BLUP is a good thing: the estimation of random effects, Stat. Sci. 6 (1) (1991) 15–32.

[74] J.M. Recla, R.F. Robledo, D.M. Gatti, C.J. Bult, G.A. Churchill, E.J. Chesler, Precise genetic mapping and integrative bioinformatics in Diversity Outbred mice reveals Hydin as a novel pain gene, Mamm. Genome 25 (5–6) (2014) 211–222.

[75] J.M. Recla, J.A. Bubier, D.M. Gatti, J.L. Ryan, K.H. Long, R.F. Robledo, N. C. Glidden, G. Hou, G.A. Churchill, R.S. Maser, Z.-W. Zhang, E.E. Young, E. J. Chesler, C.J. Bult, Genetic mapping in Diversity Outbred mice identifies a Trpa1 variant influencing late-phase formalin response, Pain 160 (8) (2019) 1740–1753.

[76] R. Petryszak, M. Keays, Y.A. Tang, N.A. Fonseca, E. Barrera, T. Burdett, A. Füllgrabe, A.M. Fuentes, S. Jupp, S. Koskinen, O. Mannion, L. Huerta, K. Megy, C. Snow, E. Williams, M. Barzine, E. Hastings, H. Weisser, J. Wright, P. Jaiswal, W. Huber, J. Choudhary, H.E. Parkinson, A. Brazma, Expression Atlas update–an integrated database of gene and protein expression in humans, animals and plants, Nucleic Acids Res. 44 (D1) (2016) D746–D752.

[77] J.H. Finger, C.M. Smith, T.F. Hayamizu, I.J. McCright, J. Xu, M. Law, D.R. Shaw, R.M. Baldarelli, J.S. Beal, O. Blodgett, J.W. Campbell, L.E. Corbani, J.R. Lewis, K. L. Forthofer, P.J. Frost, S.C. Giannatto, L.N. Hutchins, D.B. Miers, H. Motenko, K. R. Stone, J.T. Eppig, J.A. Kadin, J.E. Richardson, M. Ringwald, The mouse gene expression database (GXD): 2017 update, Nucleic Acids Res. 45 (D1) (2017) D730–d736.

[78] J.A. Blake, J.T. Eppig, J.A. Kadin, J.E. Richardson, C.L. Smith, C.J. Bult, Mouse Genome Database (MGD)-2017: community knowledge resource for the laboratory mouse, Nucleic Acids Res. 45 (D1) (2017) D723–d729.

[79] R.D. Finn, T.K. Attwood, P.C. Babbitt, A. Bateman, P. Bork, A.J. Bridge, H. Y. Chang, Z. Dosztányi, S. El-Gebali, M. Fraser, J. Gough, D. Haft, G.L. Holliday, H. Huang, X. Huang, I. Letunic, R. Lopez, S. Lu, A. Marchler-Bauer, H. Mi, J. Mistry, D.A. Natale, M. Necci, G. Nuka, C.A. Orengo, Y. Park, S. Pesseat, D. Piovesan, S.C. Potter, N.D. Rawlings, N. Redaschi, L. Richardson, C. Rivoire, A. Sangrador-Vegas, C. Sigrist, I. Sillitoe, B. Smithers, S. Squizzato, G. Sutton, N. Thanki, P.D. Thomas, S.C. Tosatto, C.H. Wu, I. Xenarios, L.S. Yeh, S.Y. Young, A.L. Mitchell, InterPro in 2017-beyond protein family and domain annotations, Nucleic Acids Res. 45 (D1) (2017) D190–d199.

[80] M. Ashburner, C.A. Ball, J.A. Blake, D. Botstein, H. Butler, J.M. Cherry, A. P. Davis, K. Dolinski, S.S. Dwight, J.T. Eppig, M.A. Harris, D.P. Hill, L. Issel-Tarver, A. Kasarskis, S. Lewis, J.C. Matese, J.E. Richardson, M. Ringwald, G. M. Rubin, G. Sherlock, Gene ontology: tool for the unification of biology. The Gene Ontology Consortium, Nat. Genet. 25 (1) (2000) 25–29.

[81] Expansion of the gene ontology knowledgebase and resources, Nucleic Acids Res. 45 (D1) (2017) D331–d338.

[82] S.A. Gagliano Taliun, P. VandeHaar, A.P. Boughton, R.P. Welch, D. Taliun, E. M. Schmidt, W. Zhou, J.B. Nielsen, C.J. Willer, S. Lee, L.G. Fritsche, M. Boehnke, G.R. Abecasis, Exploring and visualizing large-scale genetic associations by using PheWeb, Nat. Genet. 52 (6) (2020) 550–552.

[83] R.J. Kinsella, A. Kähäri, S. Haider, J. Zamora, G. Proctor, G. Spudich, J. Almeida-King, D. Staines, P. Derwent, A. Kerhornou, P. Kersey, P. Flicek, Ensembl BioMarts: a hub for data retrieval across taxonomic space, Database (2011) 2011.

[84] G.M. Davey, W.R. Heath, R. Starr, SOCS1: a potent and multifaceted regulator of cytokines and cell-mediated inflammation, Tissue Antigens 67 (1) (2006) 1–9.

[85] E. Saint-Germain, L. Mignacca, M. Vernier, D. Bobbala, S. Ilangumaran, G. Ferbeyre, SOCS1 regulates senescence and ferroptosis by modulating the expression of p53 target genes, Aging 9 (10) (2017) 2137–2162.

[86] J.K.M. Lim, A. Delaidelli, S.W. Minaker, H.-F. Zhang, M. Colovic, H. Yang, G. L. Negri, S. von Karstedt, W.W. Lockwood, P. Schaffer, G. Leprivier, P. H. Sorensen, Cystine/glutamate antiporter xCT (SLC7A11) facilitates oncogenic RAS transformation by preserving intracellular redox balance, Proc. Natl. Acad. Sci. Unit. States Am. 116 (19) (2019) 9433.

[87] S.C. Lu, Regulation of glutathione synthesis, Mol. Aspect. Med. 30 (1–2) (2009) 42–59.

[88] A. Ryo, F. Suizu, Y. Yoshida, K. Perrem, Y.C. Liou, G. Wulf, R. Rottapel, S. Yamaoka, K.P. Lu, Regulation of NF-kappaB signaling by Pin1-dependent prolyl isomerization and ubiquitin-mediated proteolysis of p65/RelA, Mol. Cell. 12 (6) (2003) 1413–1426.

[89] Z. Peng, E. Geh, L. Chen, Q. Meng, Y. Fan, M. Sartor, H.G. Shertzer, Z.G. Liu, A. Puga, Y. Xia, Inhibitor of kappaB kinase beta regulates redox homeostasis by controlling the constitutive levels of glutathione, Mol. Pharmacol. 77 (5) (2010) 784–792.

[90] Q. Meng, Z. Peng, L. Chen, J. Si, Z. Dong, Y. Xia, Nuclear Factor-κB modulates cellular glutathione and prevents oxidative stress in cancer cells, Canc. Lett. 299 (1) (2010) 45–53.

[91] A. Ulc, A. Zeug, J. Bauch, S. van Leeuwen, T. Kuhlmann, C. Ffrench-Constant, E. Ponimaskin, A. Faissner, The guanine nucleotide exchange factor Vav3 modulates oligodendrocyte precursor differentiation and supports remyelination in white matter lesions, Glia 67 (2) (2019) 376–392.

[92] S. Roth, H. Bergmann, M. Jaeger, A. Yeroslaviz, K. Neumann, P.-A. Koenig, C. Prazeres da Costa, L. Vanes, V. Kumar, M. Johnson, M. Menacho-Márquez, B. Habermann, V.L. Tybulewicz, M. Netea, X.R. Bustelo, J. Ruland, Vav proteins are key regulators of Card9 signaling for innate antifungal immunity, Cell Rep. 17 (10) (2016) 2572–2583.

[93] N. Marui, M.K. Offermann, R. Swerlick, C. Kunsch, C.A. Rosen, M. Ahmad, R. W. Alexander, R.M. Medford, Vascular cell adhesion molecule-1 (VCAM-1) gene transcription and expression are regulated through an antioxidant-sensitive mechanism in human vascular endothelial cells, J. Clin. Invest. 92 (4) (1993) 1866–1874.

[94] E. Astarci, A. Sade, I. Cimen, B. Savaş, S. Banerjee, The NF-κB target genes ICAM-1 and VCAM-1 are differentially regulated during spontaneous differentiation of Caco-2 cells, FEBS J. 279 (16) (2012) 2966–2986.

[95] T.L. Deem, J.M. Cook-Mills, Vascular cell adhesion molecule 1 (VCAM-1) activation of endothelial cell matrix metalloproteinases: role of reactive oxygen species, Blood 104 (8) (2004) 2385–2393.

[96] L. Li, B.R. Ernsting, M.J. Wishart, D.L. Lohse, J.E. Dixon, A family of putative tumor suppressors is structurally and functionally conserved in humans and yeast, J. Biol. Chem. 272 (47) (1997) 29403–29406.

[97] L. Li, M. Ljungman, J.E. Dixon, The human Cdc14 phosphatases interact with and dephosphorylate the tumor suppressor protein p53, J. Biol. Chem. 275 (4) (2000) 2410–2414.

[98] M.T. Paulsen, A.M. Starks, F.A. Derheimer, S. Hanasoge, L. Li, J.E. Dixon, M. Ljungman, The p53-targeting human phosphatase hCdc14A interacts with the Cdk1/cyclin B complex and is differentially expressed in human cancers, Mol. Canc. 5 (1) (2006) 25.

[99] M. Lacroix, R. Riscal, G. Arena, L.K. Linares, L. Le Cam, Metabolic functions of the tumor suppressor p53: implications in normal physiology, metabolic disorders, and cancer, Mol Metab 33 (2020) 2–22.

[100] P. Jiang, W. Du, X. Wang, A. Mancuso, X. Gao, M. Wu, X. Yang, p53 regulates biosynthesis through direct inactivation of glucose-6-phosphate dehydrogenase, Nat. Cell Biol. 13 (3) (2011) 310–316.

[101] A.M. Alanazi, G.A.E. Mostafa, A.A. Al-Badr, Chapter two - glutathione, in: H.G. Brittain (Ed.), Profiles of Drug Substances, Excipients and Related Methodology, Academic Press2015, pp. 43-158.

[102] D. Liu, Y. Xu, p53, oxidative stress, and aging, Antioxid Redox Signal 15 (6) (2011) 1669–1678.

[103] K.M. Kim, S.H. Ki, Chapter 28 - nrf2: a key regulator of redox signaling in liver diseases, in: P. Muriel (Ed.), Liver Pathophysiol, Academic Press, Boston, 2017, pp. 355–374.

[104] J. Fujii, J.-I. Ito, X. Zhang, T. Kurahashi, Unveiling the roles of the glutathione redox system in vivo by analyzing genetically modified mice, J. Clin. Biochem. Nutr. 49 (2) (2011) 70–78.

[105] E. Habib, K. Linher-Melville, H.-X. Lin, G. Singh, Expression of xCT and activity of system xc− are regulated by NRF2 in human breast cancer cells in response to oxidative stress, Redox Biol 5 (2015) 33–42.

[106] P. Koppula, Y. Zhang, L. Zhuang, B. Gan, Amino acid transporter SLC7A11/xCT at the crossroads of regulating redox homeostasis and nutrient dependency of cancer, Cancer Commun 38 (1) (2018) 12.

[107] H. Sasaki, H. Sato, K. Kuriyama-Matsumura, K. Sato, K. Maebara, H. Wang, M. Tamba, K. Itoh, M. Yamamoto, S. Bannai, Electrophile response element-mediated induction of the cystine/glutamate exchange transporter gene expression, J. Biol. Chem. 277 (47) (2002) 44765–44771.

[108] M. Conrad, H. Sato, The oxidative stress-inducible cystine/glutamate antiporter, system x (c) (-) : cystine supplier and beyond, J. Amino Acids 42 (1) (2012) 231–246.

[109] A.J.L. Chia, C.E. Goldring, N.R. Kitteringham, S.Q. Wong, P. Morgan, B.K. Park, Differential effect of covalent protein modification and glutathione depletion on the transcriptional response of Nrf2 and NF-κB, Biochem. Pharmacol. 80 (3) (2010) 410–421.

[110] M. Fujimoto, T. Naka, SOCS1, a negative regulator of cytokine signals and TLR responses, in human liver diseases, Gastroenterol Res Pract (2010) 470468.

[111] P.E. Collins, I. Mitxitorena, R.J. Carmody, The ubiquitination of NF-κB subunits in the control of transcription, Cells 5 (2) (2016) 23.

[112] J. Strebovsky, P. Walker, R. Lang, A.H. Dalpke, Suppressor of cytokine signaling 1 (SOCS1) limits NFκB signaling by decreasing p65 stability within the cell nucleus, FASEB J 25 (3) (2011) 863–874.

[113] The Jackson Laboratory, Mouse Genome Database (MGD), Mouse Genome Informatics, 2020.

[114] J.C. Marine, D.J. Topham, C. McKay, D. Wang, E. Parganas, D. Stravopodis, A. Yoshimura, J.N. Ihle, SOCS1 deficiency causes a lymphocyte-dependent perinatal lethality, Cell 98 (5) (1999) 609–616.

[115] A. Kempinska-Podhorodecka, E. Wunsch, P. Milkiewicz, E. Stachowska, M. Milkiewicz, The association between SOCS1-1656g>A polymorphism, insulin resistance and obesity in nonalcoholic fatty liver disease (NAFLD) patients, J. Clin. Med. 8 (11) (2019) 1912.

[116] C.W. Schmidt, Diversity outbred: a new generation of mouse model, Environ. Health Perspect. 123 (3) (2015) A64–A67.

[117] M. Irie, T. Sohda, A. Anan, A. Fukunaga, K. Takata, T. Tanaka, K. Yokoyama, D. Morihara, Y. Takeyama, S. Shakado, S. Sakisaka, Reduced glutathione suppresses oxidative stress in nonalcoholic fatty liver disease, Euroasian J. Hepato-Gastroenterol. 6 (1) (2016) 13–18.

[118] D. Han, N. Hanawa, B. Saberi, N. Kaplowitz, Mechanisms of Liver Injury. III. Role of glutathione redox status in liver injury, Am. J. Physiol. Gastrointest. Liver Physiol. 291 (1) (2006) G1–G7.

[119] L. Krugner-Higby, S. Caldwell, K. Coyle, E. Bush, R. Atkinson, V. Joers, The effects of diet composition on body fat and hepatic steatosis in an animal (Peromyscus californicus) model of the metabolic syndrome, Comp. Med. 61 (1) (2011) 31–38.

[120] L.B. Meakin, T. Sugiyama, G.L. Galea, W.J. Browne, L.E. Lanyon, J.S. Price, Male mice housed in groups engage in frequent fighting and show a lower response to additional bone loading than females or individually housed males that do not fight, Bone 54 (1) (2013) 113–117.